Charles University Prague
Faculty of Mathematics and Physics

BACHELOR THESIS

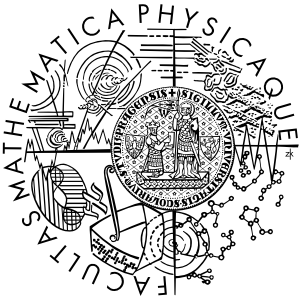

Daniel Scheirich

Testing Semiconductor Detectors Using Beam of Charged Particles

Institute of Particle and Nuclear Physics

Supervisor: Peter Kodyš, PhD.

Study programme: General Physics

2006

Univerzita Karlova v Praze
Matematicko-fyzikální fakulta

BAKALÁŘSKÁ PRÁCE

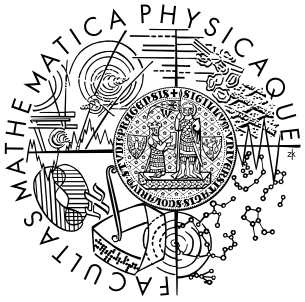

Daniel Scheirich

Testování polovodičových detektorů pomocí svazku nabitých částic

Ústav částicové a jaderné fyziky

Vedoucí bakalářské práce: RNDr. Peter Kodyš, CSc.
Studijní program: Obecná fyzika

2006

I would like to thank all the people who have introduced me into the problematics of test beams, especially to my supervisor Peter Kodyš and his colleague Zdeněk Doležal for their valuable advice, comments and very inspiring discussions. Last but not least, I would like to thank Pavel Řezníček who taught me a lot about Geant 4 and Root systems.

I declare that I wrote my bachelor thesis independently and exclusively with the use of the cited sources. I agree with lending and publishing the thesis.

Prohlašuji, že jsem svou bakalářskou práci napsal samostatně a výhradně s použitím citovaných pramenů. Souhlasím se zapůjčováním práce a jejím zveřejňováním.

In Prague, 26$^{\text{th}}$ May 2006 Daniel Scheirich

Contents

Title: Testing Semiconductor Detectors Using Beam of Charged Particles
Author: Daniel Scheirich
Department: Institute of Particle and Nuclear Physics
Supervisor: Peter Kodyš, PhD.
Supervisor's e-mail address: peter.kodys@mff.cuni.cz

Abstract: In this bachelor thesis we study in detail position resolution of test beams for which purpose Geant 4 Monte Carlo simulation has been developed. It was used in order to find the optimal geometry for January 2006 DEPFET detector test beam in DESY. Then the real geometry of the test beam was set up in the simulation and the contribution of the telescope spatial resolution and the multiple scattering to the residual distribution in DUT plane was estimated with its help. The method how to estimate that contribution using the measured data was developed as well and the results were compared. Finally the spatial resolution of several DEPFET sensors was estimated using the results of the test beam and the simulations.

Keywords: test beam, spatial resolution, simulations, Geant 4

Název práce: Testování polovodičových detektorů pomocí svazku nabitých částic
Autor: Daniel Scheirich
Katedra (ústav): Ústav částicové a jaderné fyziky
Vedoucí bakalářské práce: RNDr. Peter Kodyš, CSc.
e-mail vedoucího: peter.kodys@mff.cuni.cz

Abstrakt: v této práci detailně studujeme prostorové rozlišení polohově citlivých detektorů při testování pomocí svazků nabitých částic. Za tímto účelem byla vytvořena Geant 4 Monte Carlo simulace. Ta byla použita k nalezení optimální geometrie pro test detektoru DEPFET konaný v lednu 2006 na svazku v DESY. Poté byla do simulace zadána skutečná geometrie testu a s její pomocí byl odhadnut příspěvek prostorových rozlišení teleskopů a mnohonásobného rozptylu do distribuce reziduálů v rovině testovaného detektoru. Rovněž byla vyvinuta metoda jak odhadnout tento příspěvek z měřených dat a obdržené výsledky byly porovnány. S využitím výsledků z testu a simulací bylo odhadnuto prostorové rozlišení několika detektorů DEPFET.

Klíčová slova: testovací svazek, prostorové rozlišení, simulace, Geant 4

1 Introduction

In high energy physics the age of bubble chambers has passed away a long time ago. Nowadays, fast and a fully electronic output is expected from the tracking detectors used in particle physics experiments. The tool has changed but its purpose remains the same – it must be able to determine tracks of charged particles with a precision good enough to measure their momentum and to reconstruct vertices of secondary interactions. It means that the tracking system must measure about ten points of the track with accuracy in order of ten micrometers for outer points and in order of ones near the primary interaction vertex. For this purpose layers of silicon detectors are often used.

When a new silicon tracking detector is being developed it has to be tested and its characteristic must be measured in a laboratory. One of the variety of tests that can be conducted on a new detector prototype is a test in charged particle beam – so called test beam. One of the most important characteristic that can be measured in the test beam is the position resolution of the tested device. If a low energy electron beam (≈ 5 GeV) is used a multiple scattering in detectors and dead material can negatively influence the accuracy of measurements. Hence it is useful to make Monte Carlo simulations first in order to find the best test beam layout and to predict an influence of the multiple scattering, what was the main goal of this bachelor thesis.

It is concentrated mostly on the GEANT 4 simulation of DEPFET test beam that took place in January 2006 in DESY, but small part is devoted to the development of some theoretical methods. Using the results of this thesis the geometry of DEPFET test beam was chosen and after the real data was taken it was used to determine the spatial resolution of DEPFET sensors.

2 Test beam of silicon detectors

2.1 Silicon tracking detectors

Silicon as a material has several unique properties that make it suitable for use in high energy physics. It has a relatively low energy needed for creation of electron-hole pair (≈ 3.36 eV) and in combination with its high density (in comparison with gases) it allows to make a thin detector that creates a measurable signal but minimize the number of δ-electrons. Since read-out and front-and electronics is based on the same silicon technology it can be integrated in the same wafer.

Silicon tracking detectors are able to measure a position where a particle track intersects the detector wafer. There are two basic types of the silicon tracking detectors: the micro-strip detectors and pixel detectors.

A detection cell of the first ones consists of a thin $p+$ strip in n silicon bulk (or vice versa). From the top side the strip is covered with aluminium that is contacted to the read-out electronics. The backplane of silicon bulk is also covered with an aluminum electrode. Through the aluminium strips and the backplane a p-n junction between the n and p type of silicon is connected to a reverse bias voltage V_{bias} that extends the depleted area of the p-n junction to the almost whole detector bulk. The particle that passes through the depleted silicon wafer creates the electron-hole pairs. Electrons drift to the nearest strips where create

a signal that is processed by read-out electronics. One wafer is position sensitive only in one dimension hence there has to be two wafers in order to have a two dimensional resolution. Another way is to make strips on both sides of the wafer, each side for one axis.

The pixel detectors have square or rectangular cells (pixels) hence they have a two dimensional resolution a priori. Beside that the physical principe is similar. The pixel detectors have usually finer granularity and lower noise than the micro-strip ones do, hence they are usually placed near to the primary interaction vertex in high energy physics experiments. This innermost part of tracking system is called the vertex detector.

This thesis is concentrated on tests of the prototype of a new pixel detector called DEPFET [11] (DEPleted Field Effect Transistor). DEPFET structure integrates amplifying transistor into a fully depleted bulk. The signal charge is collected to the internal gate of the transistors. Due to an excellent noise performance of this sensor it can be made very thin (50 μm) without loss of efficiency. The 25×25 μm pixels guarantee a binary resolution of ≈ 7 μm and an analog interpolation can significantly improve this value. DEPFET detectors are one of the candidates for the vertex detector for planned International Linear Collider (ILC).

2.2 Basic concepts

When a new tracking detector prototype is manufactured it has to be tested in a laboratory in order to measure its parameters. Tests in a charged particle beam (so called test beams) are the way how to measure detector characteristics in conditions similar to ones in a real particle experiment. A tested device (so called Device Under Test or DUT) is placed in the charged particle beam (electron, pion or proton beam) and a response of the detector is measured. A lot of different characteristics can be measured, but it is not a goal of this thesis to discuss them all. Since the thesis is concentrated mostly on the position resolution of the test beam let us summarize here some basic definitions connected to this topic.

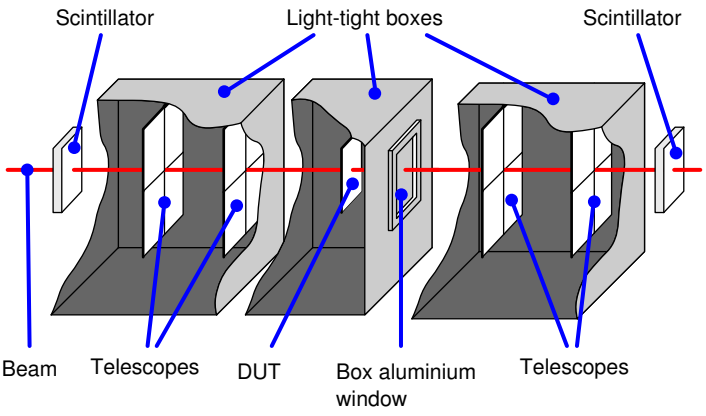

Figure 1: Typical setup of a test beam. Detectors must be placed in boxes since they are light sensitive. Telescopes are well known tracking detectors that are used in order to determine a particle track. Scintillators are used as a trigger. If there is a signal in both scintillators the detectors are read out.

Multiple scattering: When a charged particle passes through matter it is deflected in many small-angle scatters mostly due to Coulomb scattering from nuclei in material. Hence the particle leaves a layer of material in a different direction than it has entered into. The scatter angle θ is an angular displacement of the particle track entering and leaving the material. We can also define the projected scatter angle θ_{plane} as the angular displacement of these tracks projected to a certain plane.

According to Review of Particle Physics [1] the projected scatter angles are distributed according to Molière distribution, but it is sufficient to use Gaussian distribution for central 98% of the projected angular distribution. The width of the Gaussian approximation θ_0 is given by formula:

$$\theta_0 = \frac{13.6\text{MeV}\, z}{\beta cp}\sqrt{\frac{x}{X_0}}\left(1 + 0.038\, \ln\left(\frac{x}{X_0}\right)\right), \tag{1}$$

where p, βc and z are the momentum, velocity and charge number and x is the thickness. Radiation length X_0 is typical for each material.

Spatial resolution: Silicon tracking detectors are able to determine a position of an intersect of the particle track and the detector wafer. An error distribution of the position is Gaussian. The widths $\sigma^y_{detector}$ (resp. $\sigma^z_{detector}$) of the error distribution is called a spatial resolution. The silicon tracking detectors usually measure two coordinates of the intersect and the resolution can be different for each coordinate. It is also dependent on position within one detection cell (inter-strip or inter-pixel position) as Kodyš describes in [2]. In this thesis we will suppose that the resolution is constant along each coordinate axes.

Residual distribution: In order to measure the spatial resolution of the tested detector, an actual position of particle intersect in the detector plane must be known. That's the reason why there are so called telescopes placed before and after the tested device as it is shown in Figure 1. The telescopes are well known tracking detectors that are used in order to determine a particle track. If there were no multiple scattering in material the track of particle would be a straight line. Hence the particle positions obtained from the telescopes are fitted with a straight line. In reality the particle is slightly scattered in each material layer that it passes through so the track more or less differs from the ideal straight line. An example of such track is shown in Figure 2. Beside the multiple scattering spatial resolution of telescopes also affects the straight line fit. In each detector plane the residual can be defined as a distance between the measured position and the position interpolated using the straight line fit (see Figure 2).

A distribution of the residuals in DUT plane is approximately Gaussian and its width $\Delta(dut)$ has several contributions:

$$\Delta^2(dut) = \Delta^2_{ms}(dut) + \Delta^2_{tel}(dut) + \sigma^2_{dut}, \tag{2}$$

where $\Delta_{ms}(dut)$ and $\Delta_{tel}(dut)$ are contributions of the multiple scattering and telescopes spatial resolutions. Note that $\Delta_{tel}(dut)$ is strongly dependent

on the test beam geometry and it isn't equal to the spatial resolution of the telescopes σ_{tel}. On other hand σ_{dut} is DUT spatial resolution since the residual distribution is calculated in DUT plane.

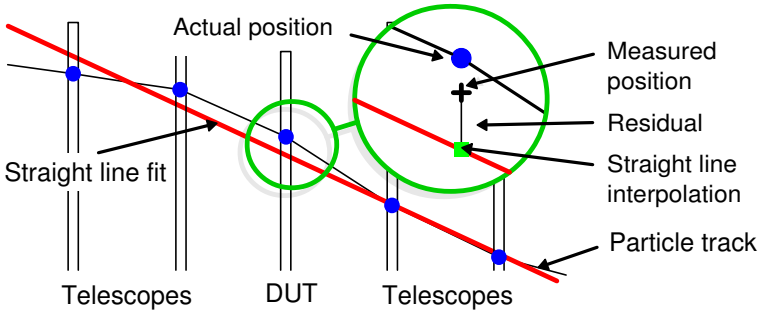

Figure 2: Example of a particle track and a straight line fitting.

Cluster size: Charged particle passing a silicon detector wafer creates electron-hole pairs along its path. The deposited charge is collected by the nearest strip or pixel and also by its neighbours. The group of strips or pixels that share the collected charge is called a cluster and the number of the strips or pixels in the cluster is called a cluster size. If the cluster size is two or more (in one dimension) the position of the intersect can be calculated using a center of gravity of the collected charge. The position can be also calculated using so called eta algorithm with better precision as it is described by Kodyš in [2].

Efficiency and purity: Velthuis et al. [4] define the efficiency $\eta_{\text{efficiency}}$ and purity η_{purity} of the detector as

$$\eta_{\text{efficiency}} = \frac{N_{\text{good clusters}}}{N_{\text{tracks}}}, \tag{3}$$

$$\eta_{\text{purity}} = \frac{N_{\text{good clusters}}}{N_{\text{clusters}}}, \tag{4}$$

where N_{track} is the number of particle tracks N_{clusters} is the number of the custers in DUT and $N_{\text{good cluster}}$ is the number of clusters that correspond to the track. If the cluster lies out of the particle track, it is assumed as a bad cluster.

Linear regression: Let $n \geq 3$ and let

$$y_i = \beta_0 + \beta_1 x_i + e_i, \text{where } i = 1, \ldots, n. \tag{5}$$

Let values e_i are distributed according to the Gaussian distribution with the mean $\mu = 0$ and the width σ. Anděl describes in [10] at page 87 how to estimate values β_0 and β_1 using the least square method. Let b_0 is the

estimation of β_0 and b_1 is the estimation of β_1. Then

$$b_1 = \frac{n\sum x_i y_i - \sum x_i \sum y_i}{n\sum x_i^2 - \left(\sum x_i\right)^2}, \tag{6}$$

$$b_0 = \frac{\sum x_i^2 \sum y_i - \sum x_i \sum x_i y_i}{n\sum x_i^2 - \left(\sum x_i\right)^2} = \bar{y} - b_1\bar{x}. \tag{7}$$

This method can be used in order to find a straight line that fits to the measured data. However there is a limitation since the values e_i must be distributed with the same σ.

Confidence interval of the estimated value $b_0 + b_1 x$ is

$$\left(b_0 + b_1 x - t_{n-2}(\alpha)s\sqrt{Q_1}, b_0 + b_1 x + t_{n-2}(\alpha)s\sqrt{Q_1}\right), \tag{8}$$

where

$$Q_1 = \frac{1}{n} + \frac{(x-\bar{x})^2}{\sum x_i^2 - n\bar{x}^2}, \tag{9}$$

$$s^2 = \frac{\sum (y_i - b_0 - b_1 x_i)^2}{n-2} \tag{10}$$

and $t_{n-2}(\alpha)$ is the critical value of the Student's distribution for the confidence level α and $n-2$ number of freedom.

The spatial resolution of DUT can be calculated using formula (2). For relativistic energies the velocity of the particle $\beta \approx 1$ and $cp \approx E$, where E is the energy of the particle. Hence according to formula (1) the angular distribution width $\theta_0 \sim 1/E$ and there is no contribution of the multiple scattering in infinite energy:

$$\Delta^2(dut) \xrightarrow[E\to\infty]{} \Delta^2_{tel}(dut) + \sigma^2_{dut}. \tag{11}$$

This can be done by plotting $\Delta^2(dut)$ vs. $1/E^2$ and making the linear extrapolation to $1/E^2 = 0$. Since in infinite energy the multiple scattering contribution is zero, the offset of the straight line equals $\Delta^2_{tel}(dut) + \sigma^2_{dut}$. An example is shown in Figure 3.

2.3 January 2006 DEPFET test beam

This paper is concentrated mostly on a simulation of DEPFET detector test beam that took place in January 2006 in DESY in Hamburg. DEPFET detector was tested in the electron beam from the DESY II synchrotron. Maximal energy of the beam was 6 GeV. Autiero et al. [5] measured the parameters of the beam. An energetic spectrum of electrons is approximately Gaussian with a slight non-gaussian tail to the lower energies. The low energy component is due to an electron scattering in the material of the beam collimator. Parameters of the spectrum are shown in Table 1.

The test beam setup is shown in Figure 4. Four telescopes were used each in its own box. The telescopes were modular PC based silicon microstrip beam telescopes, so called BATs (Bonn ATLAS Telescope). Thickness of the telescope

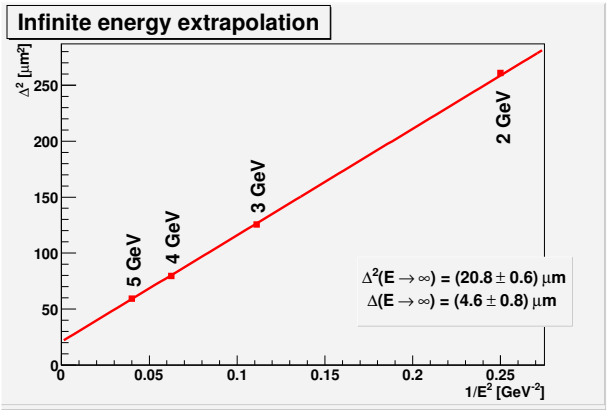

Figure 3: Example of the infinite energy extrapolation of residual distribution width. Displayed data were obtained from a simulation. $\Delta^2(E \to \infty)$ is the linear fit offset.

Mean energy [GeV]	1	2	3	4	5	6
Distribution width [GeV]	0.0462	0.0744	0.104	0.131	0.155	0.187

Table 1: Electron beam energetic spectrum parameters.

wafer is 300 μm. See Treis papers [7, 6] for more details about the telescopes. DEPFET was placed in a separated box. Thickness of the DEPFET wafer is 450 μm. Distances between detector wafers are shown in Figure 4 as well as the position of the wafers inside the boxes. The beam enters the detector modules through thin windows made of 100 μm thick aluminium foil.

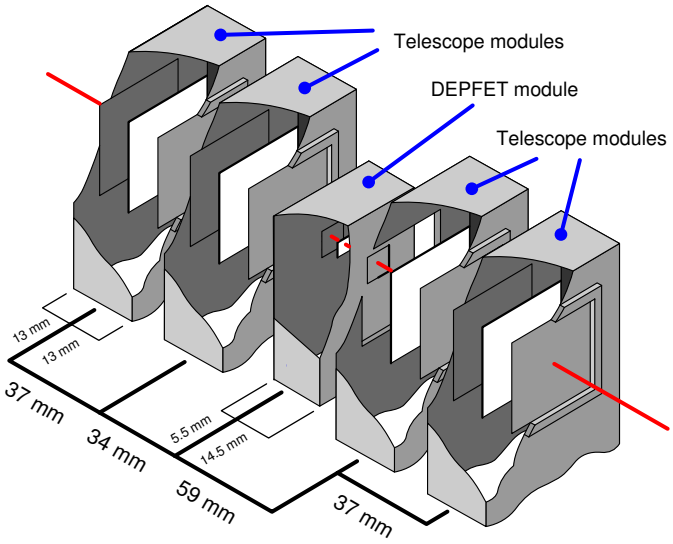

Figure 4: DEPFET test beam setup.

3 Simulations

In this section description of the simulation program is presented. It can simulate tracks of particles through detector wafers and dead material in the test beam setup. Positions, thicknesses and materials of objects in the beam can be specified

by a user as well as energy and type of particles. A homogenous magnetic field can be included to the simulation too, but this option wasn't used for DEPFET beam test simulation.

3.1 Simulation program structure

The simulation program `depfetsim` has been created in C++ using CERN Geant 4 package [8]. Geant 4 is the package of C++ libraries that contain classes for particle tracking simulations. Geant 4 libraries contain the main class called RunManager. Its instance must be created in the `Main()` function of the program. This class manages all other Geant 4 classes. Beside it Geant 4 provides many virtual classes that take care of all other aspects of the simulation. The philosophy of Geant 4 is that programmer overrides virtual methods of these classes with his own code that suits the simulation purpose. My program overrides several virtual classes provided by Geant 4:

DetectorConstruction class contains methods that create test beam detectors and place them in the coordinate system. Sensitive volumes of the detectors are specified by this class too. Dimensions, positions and materials are loaded from configuration files as well as the specification of the magnetic field.

PhysicsList class creates list of particles and physical processes used in the particle tracking.

PrimaryGeneratorAction class provides a method that is executed when tracking of primary particle is being started. This class also contains a specification of the beam: type of primary particles, dimensions of the beam and an energetic spectrum of the particles. The particles can be monoenergetic or with the Gaussian spectrum. The mean energy and Gaussian sigma are specified in the configuration file.

SensitiveWafer contains methods, that are called at the beginning and at the end of the tracking. There is also one called in each step of the tracking. These methods provide data output to ASCII files.

The program must be executed with the name of `RunManager` script as a parameter. The script contains several commands that specify number of events and whether VRML output is expected. Output to the VRML file is useful for tuning test beam geometry but should be turned off if higher number of events is simulated. See Geant 4 on-line documentation [8] in order to find more information about Geant 4 `RunManager` and its commands.

Positions of intersects and total deposited energy in each sensitive wafer are saved to an output file. A path of the particle within the sensitive wafer can be saved too. The point of intersection is calculated as a mean position of the entering and leaving point of the track. Data from this file can be converted to the Root `TTree` object [9] by macro `hits2root2.cpp`.

A web page with the program documentation was made and it is available at `http://www-ucjf.troja.mff.cuni.cz/ilc/sim`.

3.2 Data analysis macros

The simulated data were analysed in Root [9]. For this purpose a lot of macros were made that are stored in the file `analysis2.cpp`. In this section a brief description of these macros is presented:

`struct TResidual`

contains information about one particle track and methods that make the straight line fits. The fit is made using Root `TGraphErrors` object. Different weights in each telescope plane can be set.

`struct TDist:TResidual`

provides methods that can create a residual distribution or 'efficiency' histogram. Through method `loadFile()` data are loaded, methods `makePlot()` and `makeEffPlot()` create the histograms and through `save()` it can be saved to the output file. This structure is general – any telescopes resolutions and χ^2 cuts can be specified as well as any number of telescopes.

`void resDEPFET(`*parameters*`)`

function creates the residual distribution histograms in DUT or in any telescope of test beam. It creates an instance of `TDist` object and set all parameters to suit DEPFET test beam. The histograms are saved to the Root file.

`void effDEPFET(`*parameters*`)`

works the same way as `resDEPFET` but it creates 'efficiency' histogram instead of the residual distribution.

`void crDEPFET(`*parameters*`)`

works the same way as `resDEPFET` but it creates the histogram of confidence region half-length.

`void noScattering(`*parameters*`)`

creates the output file the same as from the Geant 4 simulations but the unscattered particle tracks (straight lines) are saved instead of tracks of real particles.

`struct plotHandler`

manages the histograms created by `TDist` structure. It can draw them to the specified canvas or create a table of the residual distribution widths.

`void showPlots(`*parameters*`)`

function calls methods of `plotHandler` and creates the residual distribution histograms to the canvas that can be saved to a graphic file.

`void showEffPlots(`*parameters*`)`

is the same as `showPlots` but it shows 'efficiency' histograms.

`void showEffPlots(`*parameters*`)`

is the same as `showPlots` but it shows the histograms of confidence region half-length and it makes a fit with the theoretical distribution.

`void showTelDEPFET(`*parameters*`)`

shows residual distributions in telescopes planes of DEPFET test beam.

`void extrapol(`*parameters*`)`

makes the infinite energy extrapolation of the residual ristribution width and displays the corresponding plot.

`void energyScan(`*parameters*`)`

shows an energy scan of the residual distribution width with the table of values at the bottom of the canvas. The same table is also saved to a file in LaTeX format.

`void simVsMeasure(`*parameters*`)`

has similar output as `energyScan` but any values loaded from ASCII file can be displayed in the same plot as well.

`void simVsMeaExtrapol(`*parameters*`)`

the same as `simVsMeasure` but it makes the infinite energy extrapolation of displayed values in addition.

Beside the describes functions, file `analysis2.cpp` contains many others but they are usually called by some of the described ones and shouldn't be called individually.

4 Simulation results

4.1 Model validation

In order to have a crosscheck of simulation results a passage of electrons through a single silicon wafer was simulated. An obtained angular distribution width was compared with the theoretical value given by formula (1).

The simulation was done with 1 GeV to 5 GeV electrons, 50000 events for each run. The electrons moved along x-axis perpendicular to the wafer. Positions of verticies of electron tracks were saved to an output file. Sample of 100 tracks in the x-y plane is shown in Figure 5. Only the tracks of primary particles were saved (no δ-electrons). Each track consists of single lines (steps). The track in silicon and one more step in air for each particle was saved.

Output files were analyzed by a Root macro. A tangent of the projected scatter angle θ_{plane} was calculated from the first step of the particle track after leaving the wafer. A histogram was filled with the scatter angles θ_{plane} to obtain an angular distribution.

The histogram of the projected angular distribution was fitted with a Gaussian distribution in a range given by $\pm 3/2$ of the histogram RMS since the Molière distribution has non-gaussian tails. A width σ of the fitted Gaussian in a comparison with the theoretical value θ_0 is shown in Table 2. According to Particle Physics Review [1] the accuracy of θ_0 is 11% or better for $10^{-3} < x/X_0 < 100$. The thickness of the wafer in radiation lengths of silicon is $x/X_0 \approx 3 \cdot 10^{-3}$. An example of the histogram is shown in Figure 6. An energy dependency of the Gaussian σ in a comparison with the theoretical value is shown in Figure 7.

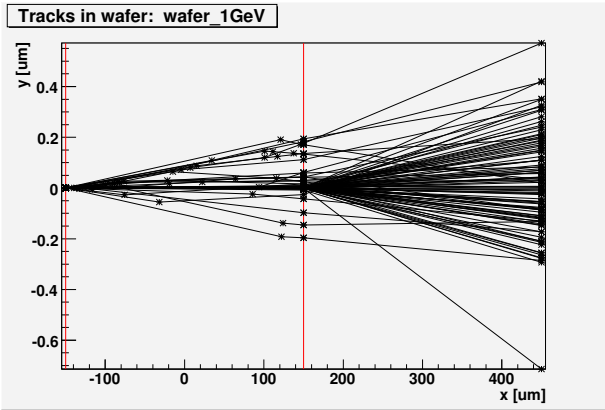

Figure 5: Example of multiple scattering in a silicon wafer. The red lines represents front and the back surface of the wafer.

	Simulation	Theory	
E [GeV]	σ [mRad]	θ_0 [mRad]	θ_0/σ
1	0.579 ± 0.002	0.602 ± 0.066	0.96
2	0.2906 ± 0.0009	0.30 ± 0.03	0.97
3	0.1955 ± 0.0006	0.20 ± 0.02	0.97
4	0.1461 ± 0.0004	0.15 ± 0.02	0.97
5	0.1172 ± 0.0003	0.12 ± 0.01	0.97

Table 2: Comparison of σ and θ_0. An error of σ is a fit parameter error calculated by Root. An uncertainty of θ_0 is 11% of the value (the worst case).

The width σ and the theoretical value θ_0 are the same in the range of their errors. From the histogram in Figure 6 it's evident that the Gaussian fit approximate well the simulated data.

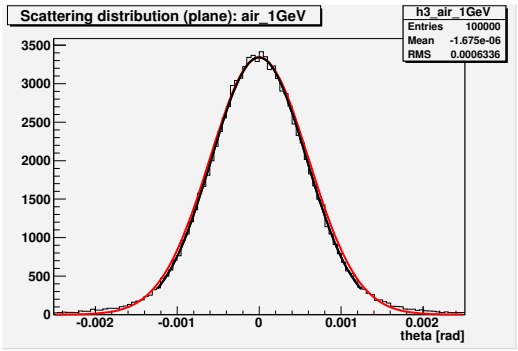

Figure 6: Example of the Gaussian fit of the projected angular distribution. The black line represents the Gaussian distribution fit, the red line represents the Gaussian part of the theoretical distribution.

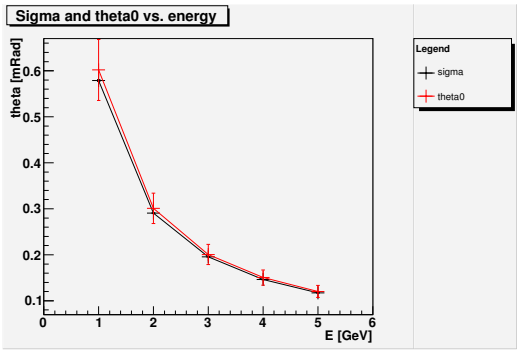

Figure 7: Energy dependency of the theoretical value of the angular distribution θ_0 and the simulated one σ.

4.2 Test beam geometry optimization

DESY II synchrotron produces 1 to 6 GeV electrons. For such energies the multiple scattering represents a quite significant contribution to the test beam residual distributions. That's the reason why simulations of possible geometries for the planned test beam were made in order to find the best one. In these simulations the spatial resolution of DUT is considered as zero since this value can't be changed by altering the test beam geometry.

The geometry of the simulation is described in Figure 8. DUT was placed in the center of the coordinate system. Two and two telescopes (TEL0 – TEL3) were placed before and behind the tested detector. The first and the last detector in the line was scintillator (SCI0 and SCI1) used for the triggering readout electronics. Centers of the detectors were situated on the x-axis. a, b, c, d, e and f are distances between the detectors centers. Results of the simulation for two different values of these distances are presented below. Telescopes and DUT wafers were made of silicon, windows were copper foils. DUT silicon wafer was covered with $0.2\,\mu$m aluminum layer. The scintillators were made of PMMA covered with $75\,\mu$m aluminium layer. Distances and window thicknesses used for the simulation are listed in Table 3. The electron beam was parallel with the x-axis. It had a square profile with a 3 mm side and it was monoenergetic and homogenous. Electrons moved in a positive direction of the x-axis.

The geometry of the simulation was similar to the one used in the real test beam, but there were some differences. In fact it wasn't a problem, because the purpose of this simulation wasn't to predict the beam test resolution but just to test a few possibilities and to compare them.

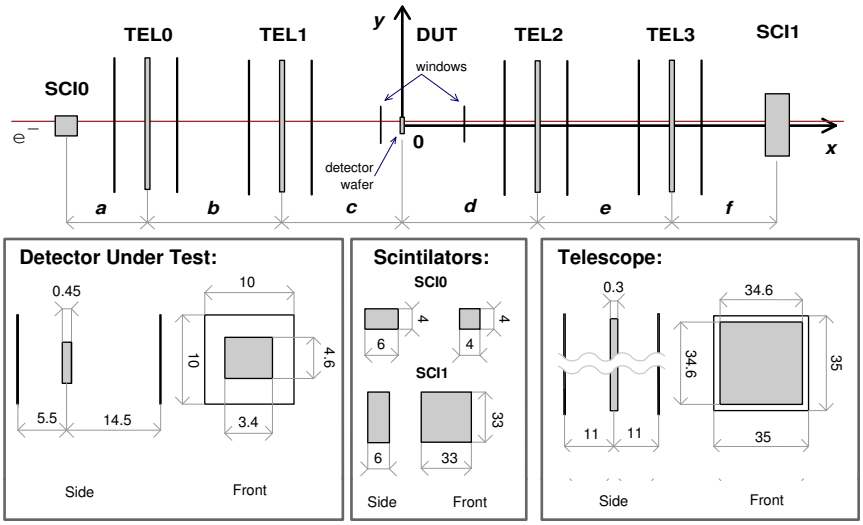

Figure 8: Geometry of the simulation. All dimensions in the figure are in millimeters.

In order to find a contribution of the telescopes spatial resolution to the residual distribution, intersects of unscattered particles were fitted firstly. Unless the telescope spatial resolution is taken into account these points will lie on a straight line. Hence the actual intersects were blurred with a Gaussian distribution in order to simulate the telescope resolutions. The Gaussian width was set to 2 μm for both coordinates. An example of the fit is shown in Figure 9.

Geometry 1		Geometry 2	
Distances	Windows	Distances	Windows
$a = f = 15$ mm $b = c = d = e = 40$ mm	1. 50 μm 2. 0 μm 3. 150 μm	$a = f = 15$ mm $b = e = 140$ mm $c = d = 40$ mm	1. 50 μm

Table 3: Distances and window thicknesses used in the simulation.

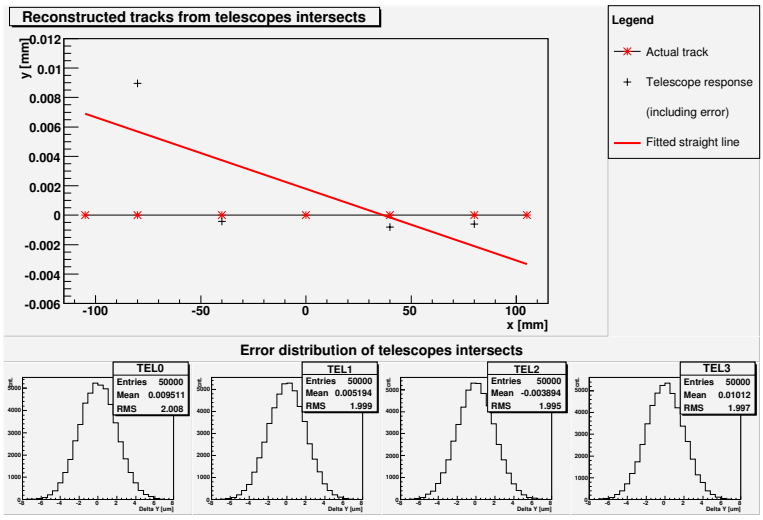

Figure 9: Example of the unscattered particle track fit in the x-y plane. The stars represents the actual intersects, the black crosses the telescopes response including the error. The residual is distance between the fitted line and the actual intersect in DUT plane.

To exclude bad fits χ^2 cuts were applied. In Table 4 there are widths of the residual distributions in the telescopes and DUT planes for the Geometry 1 and 2. In Table 5 there are the residual distributions widths in DUT plane after χ^2 cuts. Only values for the y-axis are shown in the tables since situation is the same for the z-axis. As it is evident from Tables 4 and 5 there is no significant difference between the Geometry 1 and 2. Also, χ^2 cuts don't have any significant effect on the residual distributions in DUT plane. The residual distribution width corresponding to 2 μm spatial resolution of the telescopes is approximately $\Delta_{tel}(dut) \approx 1\,\mu$m.

	Geometry 1	Geometry 2
	Δ^y_{unsct} [μm]	Δ^y_{unsct} [μm]
TEL0	1.183 ± 0.004	1.046 ± 0.003
TEL1	1.596 ± 0.005	1.677 ± 0.005
TEL2	1.592 ± 0.005	1.675 ± 0.005
TEL3	1.181 ± 0.004	1.045 ± 0.003
DUT	0.991 ± 0.006	0.991 ± 0.006

Table 4: Widths of the residual distributions in y-axis $\Delta^y_{unsct} \equiv \Delta^y_{tel}$ for the unscattered particles.

	Geometry 1	Geometry 2
χ^2 cut	$\Delta^y_{unsct}(dut)$ [μm]	$\Delta^y_{unsct}(dut)$ [μm]
100%	0.991 ± 0.006	0.991 ± 0.006
70%	0.993 ± 0.007	0.993 ± 0.007
50%	0.992 ± 0.008	0.988 ± 0.008
30%	0.99 ± 0.01	0.98 ± 0.01

Table 5: Widths of the residual distributions for the unscattered particles in DUT plane. χ^2 cuts were applied to exclude bad fits, hence the statistics were reduced to 70%, 50% and 30% of the original number of events.

After that, the simulation with 1 to 5 GeV electron beam was done. Beside telescopes spatial resolution there is also multiple scattering that significantly contributes to the residual distributions. Particles that didn't hit both scintillators were excluded from the analysis. Beside two geometries, three different window thicknesses were tested for the Geometry 1.

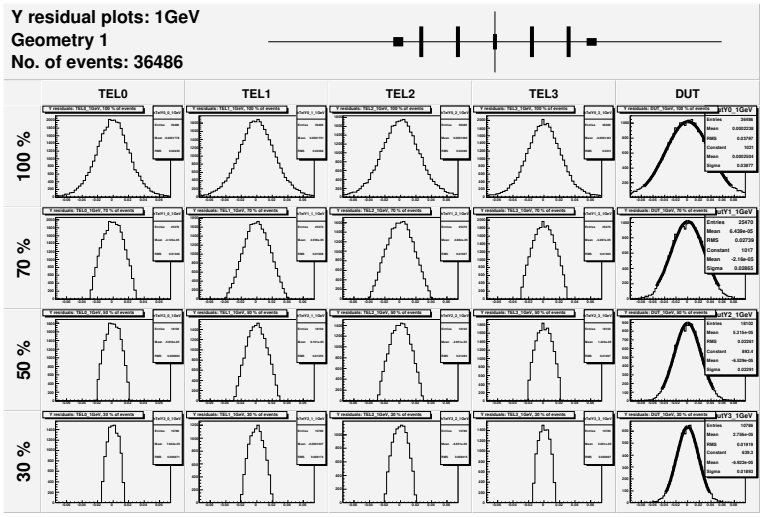

Figure 10: Example of the residual distributions of 1 GeV electrons. χ^2 cuts were applied to exclude bad fits. Note that the residual distributions in the telescopes planes are no more Gaussian after χ^2 cuts were applied.

An example of the residual distributions in the telescopes and DUT planes is shown in Figure 10. Here the χ^2 cuts play an important role in reduction of the multiple scattering influence. A comparison of two tested geometries is shown in the summary chart in Figure 11 – left. Only the widths of the residual distributions in DUT plane are shown in the figure. The thickness of the windows was 50 μm for both geometries. A comparison of the results for the different window thicknesses is shown in Figure 11 – right. The corresponding values are displayed in Table 6. Since there is a lot of numbers shown in the plots in Figure 11 there are only values with the most strict χ^2 cut in the table.

As it is evident from Figure 11 and Table 6 the Geometry 2 gives wider residual distributions in DUT plane. It's the effect of the multiple scattering, because influence of the telescopes resolution is the same for both geometries. That's the reason why in the January test beam the geometry similar to the Geometry 1 was used. Another conclusion of this simulation is that there should be used as less

dead material between the detectors as possible. Aluminium windows were used instead of copper ones in the final test beam setup since aluminium has lower proton number.

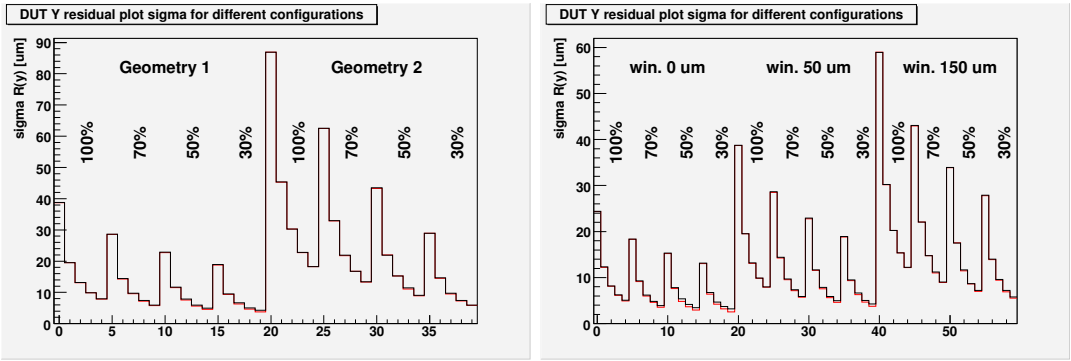

Figure 11: Comparison of the tested geometries for the electron beam. Each column represents value of the residual distribution width in DUT plane. The comparison of the Geometry 1 and 2 is shown in the left plot, the comparison of three different window thicknesses is shown in the right one. Groups of five columns labelled 100% – 30% represent the values after the corresponding χ^2 cut. In each group the leftmost column corresponds to the 1 GeV electron beam, the rightmost to the 5 GeV one. The red line represents the values for the ideal detectors, the black one correspond to the simulation with the telescope spatial resolution included.

Finally the CERN 180 GeV pion beam was simulated. Only two geometries were tested. Since 180 GeV pions have much lower multiple scattering than 5 GeV electrons, there is not expected significant dependence on the windows thickness. Values of the residual distribution width in DUT plane are tabled in Table 7. The difference between the values with the χ^2 cuts is washed out by the contribution of the telescopes spatial resolution since it is much higher then the multiple scattering. The values for Geometry 1 and 2 with the 30% χ^2 cut are the same in the range of their errors.

5 Comparison of simulations and measurements

As it is described in section 2.2 the spatial resolution of DUT can be determined using the infinite energy extrapolation even though a low energy electron beam is used. But the contribution of the telescope spatial resolution must be known since the infinite energy extrapolation reduces only the multiple scattering contribution. In our case the spatial resolution of the telescopes wasn't known very well. Analyzing results of ATLAS pixel detector test beam Treis et al. [7] estimated the residual distribution width in DUT plane to be better than 5.5 μm.

Assuming that the spatial resolution of all the telescopes was the same and that the multiple scattering does not play role since 180 GeV pion beam was used, we can estimate the spatial resolution of the telescopes using Treis result. Let the coordinate system is chosen that the position of DUT $x = 0$. According

Ideal telescopes				
	Geometry 1			Geometry 2
Thickness	0 μm	50 μm	150 μm	50 μm
E [GeV]	$\Delta_{ms}(dut)$ [μm]			
1	13.0 ± 0.1	18.8 ± 0.2	27.8 ± 0.3	28.9 ± 0.4
2	6.38 ± 0.06	9.35 ± 0.09	13.9 ± 0.1	14.5 ± 0.2
3	4.23 ± 0.04	6.30 ± 0.06	9.44 ± 0.10	9.54 ± 0.10
4	3.19 ± 0.03	4.66 ± 0.05	6.93 ± 0.07	7.29 ± 0.07
5	2.55 ± 0.03	3.75 ± 0.04	5.55 ± 0.06	5.85 ± 0.07
Telescopes resolution included				
	$\Delta_{ms+tel}(dut)$ [μm]			
1	13.2 ± 0.1	18.9 ± 0.2	27.9 ± 0.3	29.0 ± 0.4
2	6.77 ± 0.07	9.48 ± 0.09	14.0 ± 0.1	14.7 ± 0.2
3	4.67 ± 0.05	6.66 ± 0.06	9.6 ± 0.1	9.7 ± 0.1
4	3.73 ± 0.04	5.02 ± 0.05	7.21 ± 0.08	7.44 ± 0.07
5	3.20 ± 0.03	4.28 ± 0.04	5.79 ± 0.06	5.94 ± 0.06

Table 6: Residual distribution widths in DUT plane for the electron beam after 30% χ^2 cut. The first part of the table represents contribution of the multiple scattering $\Delta_{ms}(dut)$. The second part represents the contribution of both: the multiple scattering and the telescopes resolution $\Delta_{ms+tel}(dut)$. The telescopes resolution σ_{tel} was set to 2 μm. Three different thicknesses of the detector box windows were used.

Ideal telescopes		
	Geometry 1	Geometry 2
χ^2 cut	$\Delta_{ms}(dut)$ [μm]	
100%	0.215 ± 0.001	0.499 ± 0.003
70%	0.1482 ± 0.0009	0.355 ± 0.003
50%	0.1137 ± 0.0009	0.238 ± 0.002
30%	0.0956 ± 0.0010	0.133 ± 0.001
Telescopes resolution included		
	$\Delta_{ms+tel}(dut)$ [μm]	
100%	1.020 ± 0.006	1.138 ± 0.007
70%	1.025 ± 0.007	1.127 ± 0.008
50%	1.024 ± 0.009	1.132 ± 0.009
30%	1.02 ± 0.01	1.12 ± 0.01

Table 7: Widths of the residual distributions in DUT plane for 180 GeV pion beam.

to formulae (5) and (7) the residual in DUT plane can be defined as

$$res_y = b_0 - \beta_0 = \bar{y} - b_1\bar{x} - \beta_0 = \frac{1}{n}\sum(\beta_0 + \beta_1 x_i + e_i) - b_1\bar{x} - \beta_0 = \\ \beta_0 + \beta_1\bar{x} + \bar{e} - b_1\bar{x} - \beta_0 = \bar{e} + (\beta_1 - b_1)\bar{x}, \qquad (12)$$

where y_i are the measured positions of the particle in telescopes, e_i are displacements in the telescopes planes according to the error distribution, x_i are the positions of the telescopes, β_0 and β_1 are the offset and the tangent of the particle track and finally b_0 and b_1 are their estimations obtained by the least square method.

The value $\beta_1 - b_1$ is not known but for the symmetric layout of the telescopes $\bar{x} = 0$ and this value does not matter anymore. At page 70 in [10] Anděl describes

that the arithmetic mean of n Gaussian distributed values is also Gaussian distributed with the width $\tilde{\sigma}^2 = \sigma^2/n$, where σ is the width of the original Gaussian. Since there were 4 telescope planes in the beam test we can estimate the telescope resolution to be better than 11 μm.

Another way how to determine the telescopes resolution is to use a simulation. This method is described in section 5.2.

5.1 Results of January 2006 DEPFET test beam

Results of January 2006 test beam were analyzed by Velthuis et al. [4] and Kodyš [3]. In this section we summarize the Kodyš's results that were used in a comparison with the simulated ones. Beam test raw data were analyzed and the residual distributions in each telescope plane were made. The telescope in which the residual distribution is calculated was also included into the linear fit. In the fit the resolution of all the telescopes was set to 12 μm so all the points had the same weight. The central part of the distributions was fitted with a Gaussian. The residual distribution widths taken from [3] are tabled in Table 8. An example of residual distribution for 5 GeV electrons is shown in Figure 12.

	$\Delta(tel_i)$ [μm]			
	TEL0		TEL1	
E [GeV]	y-axis	z-axis	y-axis	z-axis
1	14.1 ± 0.4	13.3 ± 0.3	16.4 ± 0.6	16.7 ± 0.7
2	9.2 ± 0.1	8.8 ± 0.1	11.1 ± 0.2	10.7 ± 0.2
3	7.5 ± 0.1	7.2 ± 0.1	9.0 ± 0.1	8.7 ± 0.1
4	6.7 ± 0.1	6.5 ± 0.1	8.1 ± 0.1	7.8 ± 0.1
5	6.5 ± 0.1	6.1 ± 0.1	7.8 ± 0.1	7.4 ± 0.1
6	6.3 ± 0.0	5.9 ± 0.0	7.5 ± 0.1	7.1 ± 0.1
	TEL2		TEL3	
E [GeV]	y-axis	z-axis	y-axis	z-axis
1	13.3 ± 0.3	13.3 ± 0.3	11.9 ± 0.2	12.0 ± 0.2
2	9.7 ± 0.1	9.0 ± 0.1	8.3 ± 0.1	7.8 ± 0.1
3	8.1 ± 0.1	7.8 ± 0.1	6.9 ± 0.1	6.7 ± 0.1
4	7.6 ± 0.1	7.1 ± 0.1	6.5 ± 0.1	6.1 ± 0.1
5	7.2 ± 0.1	6.9 ± 0.1	6.1 ± 0.0	5.8 ± 0.0
6	7.1 ± 0.1	6.7 ± 0.1	6.0 ± 0.0	5.7 ± 0.0

Table 8: Widths of the residual distributions in the telescopes plane obtained from the measured data. The analysis was made by Kodyš [3].

5.2 Telescopes resolutions

Assuming that the simulation well corresponds to the reality, it can be used to estimate the telescopes resolution. An estimation of the telescopes spatial resolution was made using the residual distributions in telescopes planes for 3 GeV electrons. The telescopes spatial resolutions in the simulation were tuned so that the residual distribution widths in telescopes obtained from the simulation and measurement were the same within errors. Obtained values are shown in Table 9.

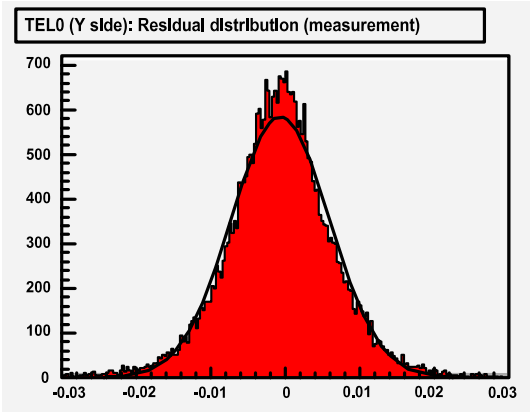

Figure 12: Example of the residual distribution in DUT plane for 5 GeV electrons obtained from the measurement.

	TEL0	TEL1	TEL2	TEL3
side Y: $\sigma^{y}_{tel_i}$ [μm]	8.7	8.2	7.8	8.4
side Z: $\sigma^{z}_{tel_i}$ [μm]	8.4	7.8	7.5	8.3

Table 9: Estimation of the telescopes spatial resolutions.

Using these values the residual distributions for all energies were calculated. A comparison of the simulated and measured widths in y-axis is shown in Table 10. The best correspondence was achieved in TEL1 plane as it is shown in Figure 13, the worst one in TEL3 plane (Figure 14). From these plots it is evident that there isn't a good correspondence between the measurement and simulation at 1 GeV. For other energies the difference is lower than 0.5 μm in every plane.

	$\Delta^{y}(tel_i)$ [μm]					
E	1 GeV	2 GeV	3 GeV	4 GeV	5 GeV	6 GeV
	Telescope plane: TEL0					
Sim	16.5 ± 0.4	9.48 ± 0.07	7.52 ± 0.04	6.67 ± 0.03	6.20 ± 0.03	5.96 ± 0.02
Mea	14.1 ± 0.4	9.2 ± 0.1	7.5 ± 0.1	6.7 ± 0.1	6.5 ± 0.1	6.3 ± 0.1
	Telescope plane: TEL1					
Sim	19.9 ± 0.7	11.1 ± 0.1	9.01 ± 0.06	8.23 ± 0.05	7.69 ± 0.04	7.50 ± 0.04
Mea	16.4 ± 0.6	11.1 ± 0.2	9.0 ± 0.1	8.1 ± 0.1	7.8 ± 0.1	7.5 ± 0.1
	Telescope plane: TEL2					
Sim	16.7 ± 0.4	9.95 ± 0.08	8.28 ± 0.05	7.68 ± 0.04	7.27 ± 0.04	7.07 ± 0.03
Mea	13.3 ± 0.3	9.7 ± 0.1	8.1 ± 0.1	7.6 ± 0.1	7.2 ± 0.1	7.1 ± 0.1
	Telescope plane: TEL3					
Sim	15.1 ± 0.3	8.65 ± 0.06	6.97 ± 0.03	6.31 ± 0.03	5.90 ± 0.02	5.66 ± 0.02
Mea	11.9 ± 0.2	8.3 ± 0.1	6.9 ± 0.1	6.5 ± 0.1	6.1 ± 0.1	6.0 ± 0.1

Table 10: Comparison of the simulated and measured widths of the residual distributions in y-axis.

5.3 Measured and simulated data comparison

In addition to the residual distribution widths for each energy, other characteristics can be simulated and compared with the measured data. Such characteristic

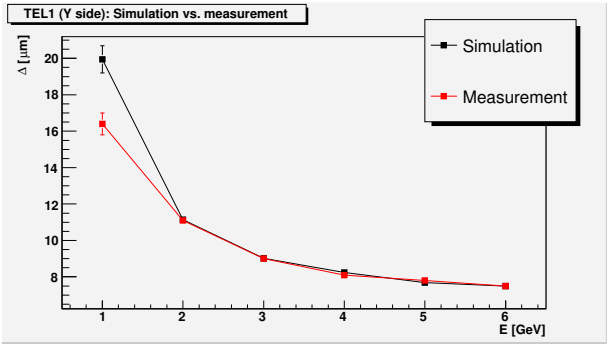

Figure 13: Example of the best correspondence between the measurement and the simulation in y-axis.

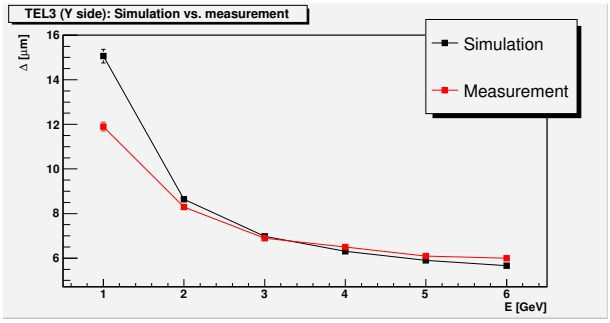

Figure 14: Example of the worst correspondence between the measurement and the simulation in y-axis.

is for instance the infinite energy extrapolation of the residual distribution width as it is described in section 2.2. It is particulary important that these values correspond to the measured ones since the infinite energy extrapolation is the way how to determine DUT spatial resolution. An example of the infinite energy extrapolation of the simulated residual distribution width in TEL1 plane is shown in Figure 15 while the same plot for the measured data is shown in Figure 16. Since at 1 GeV the simulation doesn't correspond to the measurement, these points wasn't included to the extrapolation.

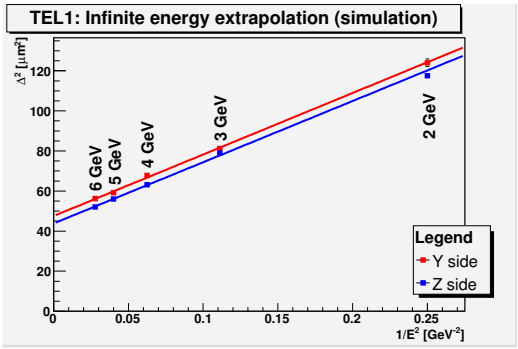

Figure 15: Example of the infinite energy extrapolation of the residual distribution width from the simulation.

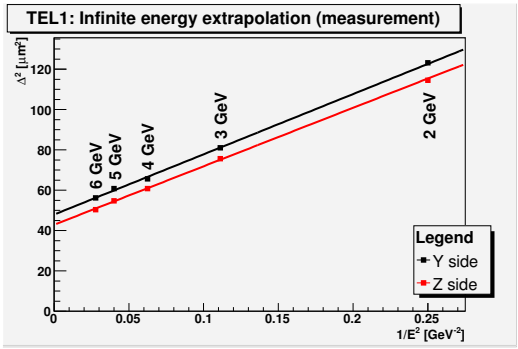

Figure 16: Example of the infinite energy extrapolation of the residual distribution width from the measurement.

A comparison of simulated and measured results in all telescopes planes is

shown in Table 11. Differences between them are lower or equal to 0.5 μm. The presented errors are statistical errors obtained by the least-square method. Beside that, there are also errors given by the accuracy of the estimated telescopes resolutions that is not known very well.

		$\Delta(tel_i, E \to \infty)$ [μm]			
		TEL0	TEL1	TEL2	TEL3
Y side	Sim	5.4 ± 0.3	6.9 ± 0.6	6.6 ± 0.6	5.2 ± 0.2
	Mea	5.9	7.1	6.7	5.6
Z side	Sim	5.2 ± 0.3	6.6 ± 0.5	6.4 ± 0.4	5.0 ± 0.2
	Mea	5.5	6.7	6.4	5.4

Table 11: Infinite energy extrapolation of the residual distribution widths in the telescopes planes.

Another interesting value that can be compared to the measured data is the confidence region of the interpolated intersect in DUT plane. The confidence interval is given by formula (8). A half-length l of the interval is a random variable and it has a distribution function:

$$f(l) = c_1 l \chi_2^2 \left(\frac{l^2}{c_2^2} \right), \tag{13}$$

where $c_1 = \frac{4\sqrt{Q_1}}{t_2(\alpha)\sigma^2}$, $c_2 = t_2(\alpha)\sigma\sqrt{\frac{Q_1}{2}}$ and χ_2^2 is the χ^2 distribution with two degrees of freedom. Here σ is the width of the error distributions in the telescopes, $t_2(\alpha)$ is the critical value of the Student's distribution and the geometrical factor Q_1 is defined by formula (9). The derivation of formula (13) is shown in Appendix B.

The function (13) has one maximum for $l = l_{MPV} = c_2$. A histogram of the confidence interval half-lengths l can be fitted with the function (13) as it is shown in Figure 17. Since the distribution of the telescopes intersects is not Gaussian due to the multiple scattering, the theoretical dependence (13) does not approximate the confidence region histogram well for higher values. Also the condition that the spatial resolution is the same for all fitted points was met neither in the real experiment nor in the simulation. But the values are similar thus it shouldn't influence the fit very much. A comparison of l_{MPV} that was got from the simulation and the measurement is shown in Table 12. The difference between the simulated and measured results is lower or equal to 0.3 μm.

Note that l_{MPV} is proportional to the width σ of the error distribution in the telescopes planes. The critical value of Student's distribution $t_2(95\%) \doteq 2.920$ and the geometrical factor Q_1 can be calculated using formula (9). For a finite energy σ consists of the contribution of the multiple scattering and the telescope spatial resolution, but the multiple scattering can be reduced using the infinite energy extrapolation:

$$\sigma = \sigma_{ms+tel} = l_{MPV} \frac{\sqrt{2}}{t_2(\alpha)\sqrt{Q_1}} \xrightarrow[E \to \infty]{} \sigma_{tel}, \tag{14}$$

where σ_{tel} is the spatial resolution of the telescopes.

This gives us method how to check that the telescopes resolutions we estimated correspond to reality since this can be done purely with the results of the

	l_{MPV} [μm]			
	Y side		Z side	
E [GeV]	Sim	Mea	Sim	Mea
2	13.5 ± 0.1	13.8 ± 0.1	13.4 ± 0.1	13.2 ± 0.1
3	11.4 ± 0.1	11.3 ± 0.1	11.0 ± 0.1	10.9 ± 0.1
4	10.5 ± 0.1	10.3 ± 0.1	10.1 ± 0.1	9.9 ± 0.1
5	9.8 ± 0.1	9.8 ± 0.1	9.5 ± 0.1	9.5 ± 0.1
6	9.7 ± 0.1	9.5 ± 0.1	9.3 ± 0.1	9.2 ± 0.1

Table 12: Maximum probable value l_{MPV} of the confidence region half-length. The presented errors are statistical errors given by the least square method. However there can be also a systematic error since theoretical formula (13) doesn't describe the distribution of confidence region half-length well for higher values. Fit procedure is then quite sensitive to the chosen fit range.

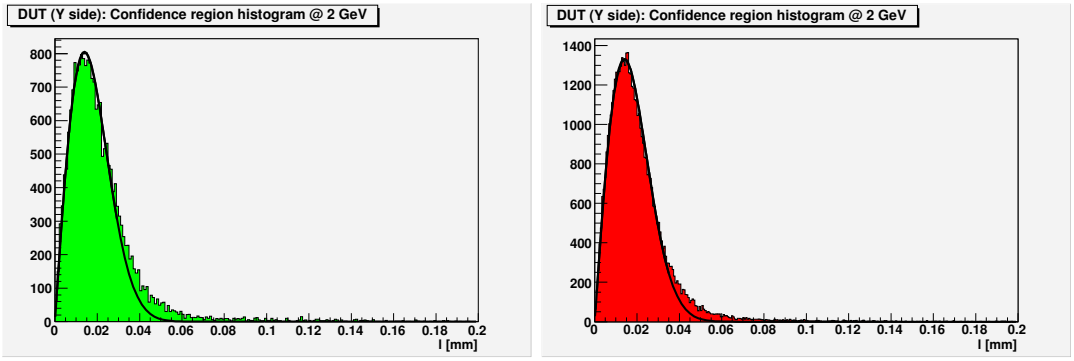

Figure 17: Example of the confidence region half-length histogram at 2 GeV. The confidence regions were calculated for confidence level 95%. The left one was created from the measured data, the right one from the simulation.

measurement. Still this method has its limits since it assumes that the spatial resolution of all the telescopes is the same. The plot σ^2 vs. $1/E^2$ was fitted with a straight line as it is shown in Figure 18.

The extrapolated values of the telescopes resolutions are

$$\begin{aligned} \sigma^y(\infty) &= \sigma^y_{tel} = (8.5 \pm 0.1)\ \mu\text{m} \quad \text{on Y side and} \\ \sigma^z(\infty) &= \sigma^z_{tel} = (8.16 \pm 0.10)\ \mu\text{m} \quad \text{on Z side.} \end{aligned}$$

The presented errors of these values are statistical ones given by the accuracy of the linear fit in the infinite energy extrapolation.

The arithmetic means of telescopes resolutions determined from the simulation (Table 9) are $\overline{\sigma}^y_{tel} = 8.3\ \mu$m and $\overline{\sigma}^z_{tel} = 8.0\ \mu$m. The difference between the extrapolated values and ones obtained from the simulation is lower or equal to 0.2 μm. Since the error of the arithmetic mean of four gaussian distributed random variables is equal to the one half of their original error (see Anděl [10]) we can very roughly estimate the lower limit of accuracy of the telescopes resolutions obtained from the simulations to be 0.4 μm.

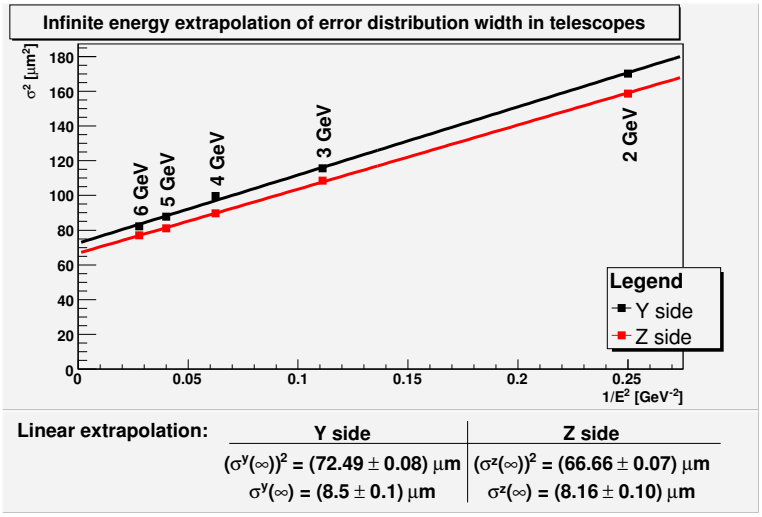

Figure 18: Infinite energy extrapolation of the error distributions width σ of the intersects in the telescopes planes. The error distribution widths were obtained from the measurement using formula (14).

5.4 Contribution of telescopes spatial resolution and multiple scattering in DUT plane

Since now we have the estimation of the telescopes resolutions, we can predict an influence of the multiple scattering and the telescopes spatial resolution in DUT plane. An example of simulated residual distributions in DUT plane is shown in Figure 19. The spatial resolution of DUT wasn't taken into account since that value should be determined from the measurement. The estimation of the telescopes spatial resolution from Table 9 was used in the simulation.

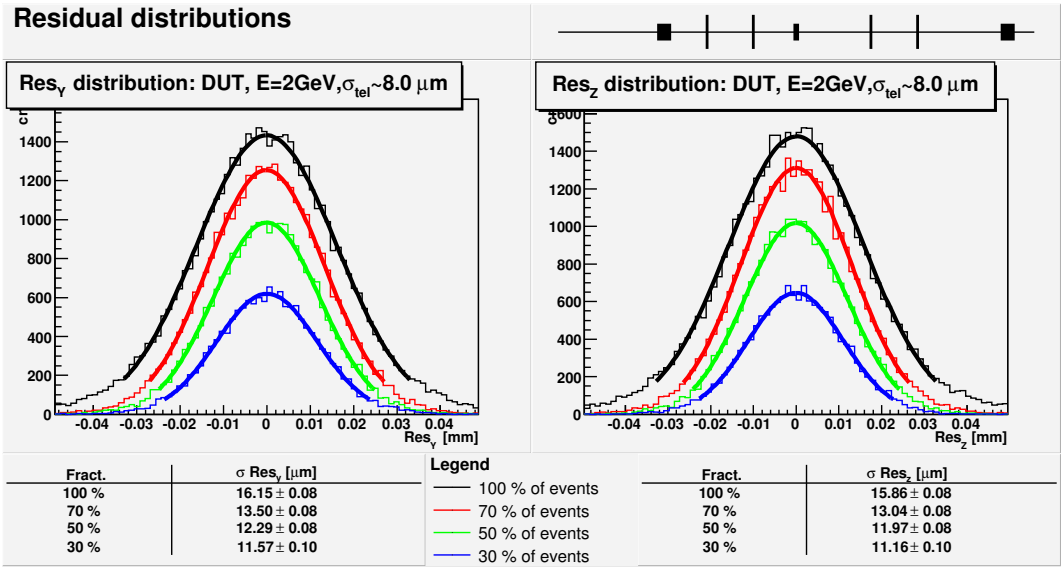

Figure 19: Example of simulated residual distributions in DUT plane at 2 GeV. Colored lines represent the residual distribution after χ^2 cut.

The residual distributions in DUT plane were simulated for energies up to 6 GeV (see Table 13 and Figure 20). The infinite energy extrapolation was made

E [GeV]	2	3	4	5	6
$\Delta^y_{ms+tel}(dut)$ [μm]	16.15 ± 0.08	11.21 ± 0.06	8.92 ± 0.05	7.70 ± 0.04	6.84 ± 0.04
$\Delta^z_{ms+tel}(dut)$ [μm]	15.86 ± 0.08	11.11 ± 0.06	8.80 ± 0.04	7.51 ± 0.04	6.67 ± 0.03

Table 13: Simulated residual distribution widths in DUT plane. The spatial resolution of DUT is not taken into account.

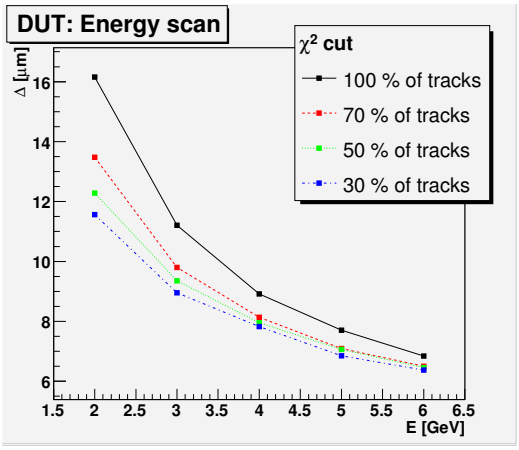

Figure 20: Residual distribution width in DUT plane. The displayed data are results of the simulation.

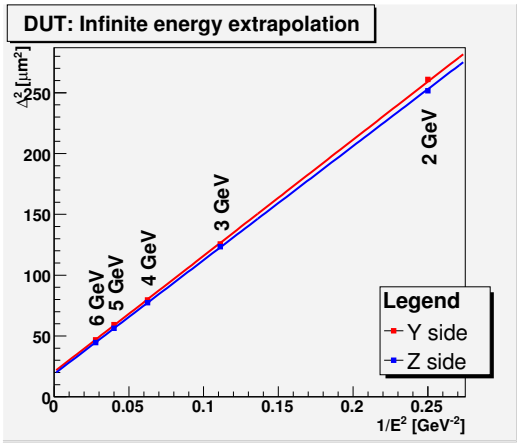

Figure 21: Infinite energy extrapolation in DUT plane. The displayed data are results of the simulation.

using these values as it is shown in Figure 21. The offset of the straight line should be equal to square of the contribution of the telescopes resolution since DUT spatial resolution wasn't involved. The extrapolated values are

$$\Delta^y_{tel+ms}(dut, E) \xrightarrow[E\to\infty]{} \Delta^y_{tel}(dut) = (4.5 \pm 0.6)\ \mu\text{m} \quad \text{and}$$
$$\Delta^z_{tel+ms}(dut, E) \xrightarrow[E\to\infty]{} \Delta^z_{tel}(dut) = (4.3 \pm 0.5)\ \mu\text{m},$$

while the contribution of the telescopes resolution obtained from the simulation of unscattered particles is

$$\Delta^y_{unsct}(dut) = (4.25 \pm 0.02)\ \mu\text{m} \quad \text{and}$$
$$\Delta^z_{unsct}(dut) = (4.06 \pm 0.02)\ \mu\text{m}.$$

In section 5.2 the method is described how to estimate the telescopes spatial resolution σ_{tel} purely from measurements (see formula (14)) assuming that it is the same for all the telescopes. If this condition is meet and if the particles are not scattered the telescopes contribution to the width of the residual distribution in DUT plane $\Delta_{tel}(dut)$ can be calculated as it is shown in Appendix B:

$$\Delta_{tel}(dut) = G(x_1, \ldots, x_n)\sigma^2_{tel} = \frac{\sum x_i^2}{n\sum x_i^2 - \left(\sum x_i\right)^2}\sigma^2_{tel}, \tag{15}$$

where $G(x_1, \ldots, x_n)$ is the geometrical factor that depends only on the telescopes positions. As it is shown in Appendix B in combination with formula (14) it gives

$$\Delta_{tel}(dut) = \frac{\sqrt{2}}{t_2(\alpha)} l_{MPV}(\infty), \tag{16}$$

where $l_{MPV}(\infty)$ is the infinite energy extrapolation of the most probable value of the confidence region half-length and $t_2(\alpha)$ is the critical value of Student's distribution with the confidence level α for that confidence region was calculated.

In order to have a crosscheck a simple simulation was made. Four telescope planes were used, the first two in distance 4 cm then 10 cm long gap and another two telescopes in distance 4 cm. DUT was placed in the middle and the spatial resolution of all the telescopes was set to 10 μm. Residual distribution of unscattered particles was calculated in DUT and since the multiple scattering wasn't involved the distribution width was $\Delta_{tel}(dut) = 5$ μm. Then DUT was shifted down the beam with the step of 1 cm and residual distributions were calculated again. Dependence of the width $\Delta_{tel}(dut)$ on DUT position x_{DUT} is shown in Figure 22. It is evident that formula (15) well describes the simulation results for unscattered particles.

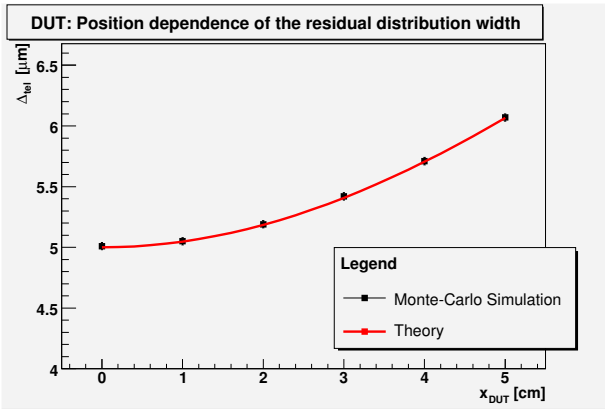

Figure 22: Dependence of the residual distribution width in DUT plane on DUT position. DUT was shifted by x_{DUT} from the central position between the telescopes. Value Δ_{tel} for $x_{DUT} = 5$ cm equals to the residual distribution width in one inner telescope.

In reality the resolutions of the telescopes aren't the same and the multiple scattering is involved. Theoretically, we can estimate the width of the error distributions σ_{tel+ms} through the maximum probable half-length l_{MPV} of the confidence interval in DUT as it is described in section 5.3, but these values can't be used in formula (15). It's because if we do it, it will be like to calculate the residual distribution width of the unscattered particles, where the new value of the error distributions width $\sigma = \sigma_{tel+ms}$ instead of the telescopes spatial resolution σ_{tel} is used in the telescopes planes. But the real particles don't have the straight tracks and this fact strongly influences calculation of residuals as it is illustrated in Figure 23. Hence the real residual distribution width $\Delta_{ms+tel}(dut)$ will be different than formula (15) predicts.

In spite of that the residual distribution in DUT can be predicted using formula (15) if the infinite energy extrapolation is used. Both the error distribution widths in the telescopes σ_{tel+ms} and the measured residual distributions in DUT $\Delta(dut, E) \equiv \Delta_{ms+tel+dut}(dut, E)$ must be extrapolated to the infinite energy (see formula (14) in section 5.2 and formula (11) in section 2.2). Since the contribution

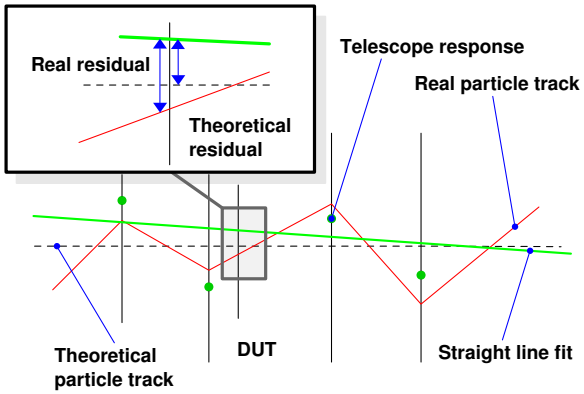

Figure 23: Calculation of residuals. Real particle track is represented by the red line. Due to the telescopes spatial resolution the intersects in the telescopes are shifted (green points) and these points are fitted with the straight line (green line). Formula (15) assumes, that the particle track is straight (dashed line) hence the theoretical residual is different than the real one (upper left corner).

		$\Delta^y_{tel}(dut)$ [μm]	$\Delta^z_{tel}(dut)$ [μm]
Measurement	Prediction by formula (15)	4.32 ± 0.05	4.15 ± 0.05
Simulation	Infinite energy extrapolation	4.5 ± 0.6	4.3 ± 0.5
	Unscattered particles	4.25 ± 0.02	4.06 ± 0.02

Table 14: Comparison of the telescopes contribution to the residual distribution width in DUT plane obtained by the three different methods.

of multiple scattering was reduced in the extrapolated values:

$$\begin{aligned} \sigma_{ms+tel}(E) &\xrightarrow[E\to\infty]{} \sigma_{tel}, \\ \Delta(dut, E) &\xrightarrow[E\to\infty]{} \Delta(dut, \infty) = \Delta_{tel+dut}(dut), \end{aligned}$$

the spatial resolution of DUT σ_{dut} can be calculated according to formula (2)

$$\begin{aligned} \sigma_{dut} &= \sqrt{(\Delta(dut,\infty))^2 - (\Delta_{tel}(dut))^2} = \\ &= \sqrt{(\Delta(dut,\infty))^2 - G(x_1,\ldots,x_n)\sigma^2_{tel}} = \\ &= \sqrt{(\Delta(dut,\infty))^2 - \frac{2(l_{MPV}(\infty))^2}{(t_2(\alpha))^2}}. \end{aligned} \tag{17}$$

Note that this can be done purely with the results of measurements. Since we have both the results of the measurements and also the results of the simulations it is an opportunity to check this method. In section 5.3 we have estimated the telescopes resolutions $\sigma^y_{res} = (8.5 \pm 0.1)$ μm and $\sigma^z_{res} = (8.16 \pm 0.10)$ μm from the infinite energy extrapolation of $\sigma_{ms+tel}(E)$. Using formula (15) their contribution to the residual distribution width in DUT plane was calculated. The predicted values in comparison with ones obtained from the infinite energy extrapolation of the residual distribution width and ones from the simulation of unscattered particles are shown in Table 14. The difference between these values is lower than 0.3 μm that shows a good accuracy of this method.

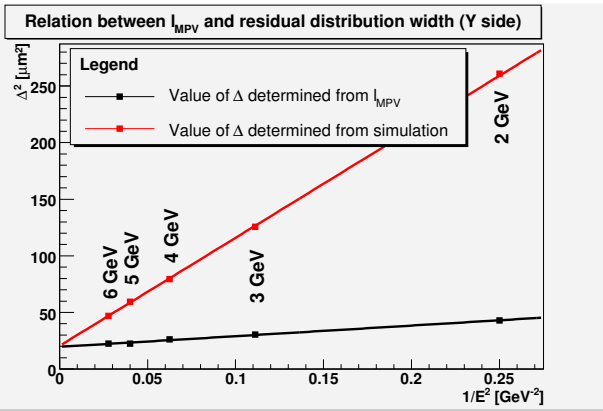

Figure 24: Comparison of squares of the formal $\Delta_{formal}(dut, E)$ and simulated $\Delta_{tel+ms}(dut)$ contribution of telescopes spatial resolution and multiple scattering to the residual distribution width in DUT plane vs. inverse square of energy. The formal value $\Delta_{formal}(dut, E)$ was calculated from l_{MPV} using formula (16).

A correction of formula (16) for finite energy can be made using simulations. Formal values of the residual distribution widths $\Delta_{formal}(dut, E)$ were calculated from the maximal probable half-length of the confidence interval $l_{MPV}(E)$ using formula (16) for finite energy. The squares of these values vs. the inverse square of energy $1/E^2$ in comparison width the squares of the simulated residual distribution widths $\Delta^2_{ms+tel}(dut)$ are plotted in Figure 24. The values were fitted with straight lines with the slope

$$\begin{aligned} a_1^y &= (93.8 \pm 0.4)\ \mu\text{m}^2\text{GeV}^2, \\ a_1^z &= (98.7 \pm 0.4)\ \mu\text{m}^2\text{GeV}^2, \qquad \text{for the formal values } \Delta_{formal}(dut, E), \\ a_2^y &= (954 \pm 7)\ \mu\text{m}^2\text{GeV}^2, \\ a_2^z &= (937 \pm 7)\ \mu\text{m}^2\text{GeV}^2, \qquad \text{for the simulated values } \Delta_{tel+ms}(dut, E). \end{aligned}$$

Using these values the telescopes and multiple scattering contribution to the residual distribution width can be calculated as

$$\Delta_{tel+ms}(dut, E) = \sqrt{\frac{2(l_{MPV}(E))^2}{(t_2(\alpha))^2} + \frac{a_2 - a_1}{E^2}}, \tag{18}$$

that can be rewritten for known values of a_1, a_2 and for confidence level $\alpha = 95\%$:

$$\begin{aligned} \Delta^y_{tel+ms}(dut, E) &= \sqrt{\frac{(l^y_{MPV}(E))^2}{4.26} + \frac{860.7}{E^2}}, \\ \Delta^z_{tel+ms}(dut, E) &= \sqrt{\frac{(l^z_{MPV}(E))^2}{4.26} + \frac{839.0}{E^2}}, \end{aligned} \tag{19}$$

where $l^y_{MPV}(E)$ and $l^z_{MPV}(E)$ are in micrometers and E in GeV. Note that formula (19) is geometry dependent and it can be used only for the exactly same test beam layout as one used in January 2006 in DESY.

5.5 Resolution and efficiency of DUT

Analysis of data measured by DEPFET detector that was used as DUT in January 2006 test beam was made by Velthuis et al. [4]. Several different matrices

were measured. Their pixel size is listed in Table 15. Preliminary values of the residual distribution widths in DUT extrapolated to infinite energy are listed in Table 16. The contribution of the telescope resolution $\Delta_{tel}(dut) \equiv \Delta_{unsct}(dut)$ was quadratically subtracted from the measured values:

$$\sigma_{dut} = \sqrt{\Delta(dut, \infty))^2 - (\Delta_{tel}(dut))^2}. \quad (20)$$

Obtained spatial resolutions of DEPFET are shown in Table 17.

hybrid	pixel size [μm $\times$ μm]
2A	33×23.75
1A	33×23.75
1B	36×22
Mun1	36×22
GCG	36×28.5

Table 15: Pixel size of DEPFET sensors.

hybrid	$(\Delta^y(dut, \infty))^2$ [μm^2]	$(\Delta^z(dut, \infty))^2$ [μm^2]
2A	65 ± 1	37.9 ± 0.9
1A	54	38
1B	54	46
Mun1	76	44
GCG	59	35

Table 16: Squares of the measured residual distribution widths in DUT extrapolated to infinite energy. Data were taken from [4].

hybrid	σ^y_{dut} [μm]	σ^z_{dut} [μm]
2A	6.85 ± 1	4.63 ± 0.9
1A	6.0	4.6
1B	6.0	5.3
Mun1	7.6	5.2
GCG	6.4	4.3

Table 17: Resolution of DEPFET.

Another important characteristics of DUT are its efficiency and purity. In order to find the number of good clusters $N_{\text{goodclusters}}$ the region of interest (ROI) is defined where hits are accepted. Due to the multiple scattering it can happen that the hit lies outside of the region of interest but should be accepted as a good hit. Consequently the efficiency $\eta_{\text{efficiency}}$ and the purity η_{purity} fractions are lower than they should be. The fraction of tracks that intersect the region of interest can be determined from the simulation. Dependence of this fraction on the region of interest size at 2 GeV is shown in Figure 25. In fact it is an integral of the distribution of residual sizes $|Res|$. The size of ROI for that 99% of hits are accepted ($\text{ROI}_{99\%}$) was calculated for each energy and χ^2 cut and is shown in Figure 26 and Table 18.

Note that there is a quite big gap between the values without any χ^2 cut and those with one. It is caused by the non-gaussian tails in the residual distributions. Even not very strict restriction on χ^2 can cut off these tails and significantly reduce the critical size of the region of interest $\text{ROI}_{99\%}$.

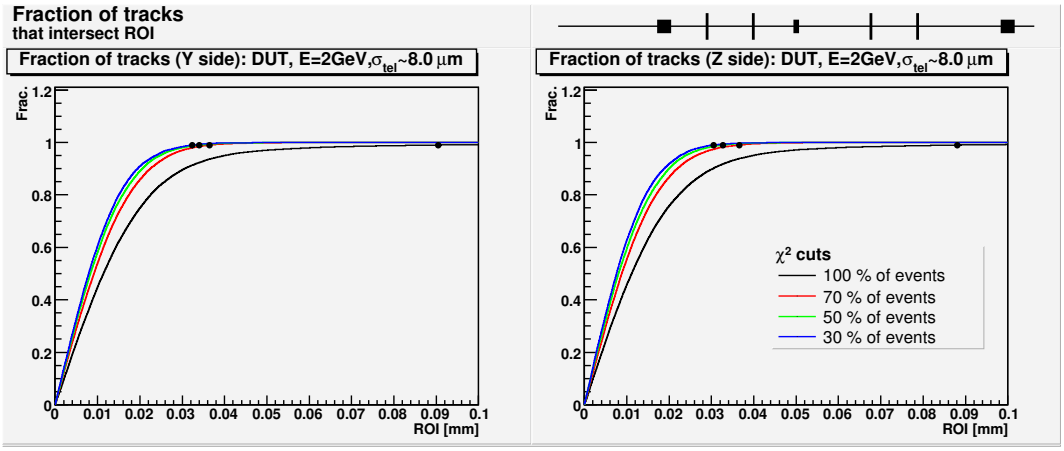

Figure 25: Dependence of the fraction of tracks that intersects ROI on its size at 2 GeV. Black points represent ROI size for that 99% of hits were accepted. There are more colored histograms in the plot, each represents different χ^2 cut.

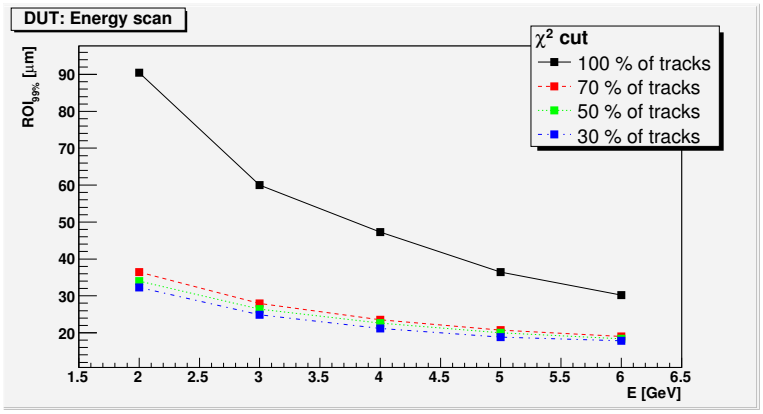

Figure 26: Size of the region of interest for that 99% of hits is accepted.

χ^2 cut	$\mathrm{ROI}^{y}_{99\%}$ [μm]				
	2 GeV	3 GeV	4 GeV	5 GeV	6 GeV
100%	90.42 ± 0.03	60.06 ± 0.03	47.26 ± 0.03	36.42 ± 0.03	30.24 ± 0.03
70%	36.48 ± 0.03	27.96 ± 0.03	23.52 ± 0.03	20.68 ± 0.03	19.02 ± 0.03
50%	34.00 ± 0.03	26.44 ± 0.03	22.62 ± 0.03	19.96 ± 0.03	18.38 ± 0.03
30%	32.32 ± 0.03	24.86 ± 0.03	21.18 ± 0.03	18.82 ± 0.03	17.86 ± 0.03
	$\mathrm{ROI}^{z}_{99\%}(z)$ [μm]				
100%	88.04 ± 0.03	60.42 ± 0.03	45.90 ± 0.03	36.04 ± 0.03	31.64 ± 0.03
70%	36.52 ± 0.03	27.32 ± 0.03	23.02 ± 0.03	20.70 ± 0.03	18.70 ± 0.03
50%	32.74 ± 0.03	25.56 ± 0.03	21.68 ± 0.03	19.48 ± 0.03	18.20 ± 0.03
30%	30.54 ± 0.03	24.22 ± 0.03	21.02 ± 0.03	19.02 ± 0.03	17.98 ± 0.03

Table 18: Size of the region of interest for that 99% of hits are accepted.

6 Conclusion

The test beam simulation program has been created using GEANT 4 package. It computes positions and energy loses in sensitive detectors in the test beam but it also takes into account dead material. The geometry of the beam test can be set up in configuration files hence many different test beam layouts can be simulated

without need to recompile the program. It allows to simulate various particles with a Gaussian energetic spectrum and a homogenous magnetic field can be included too. In November and December 2005 the program was used in order to find an optimal layout for DEPFET test beam that had been planned for January 2006 on DESY II synchrotron which provides 1 to 6 GeV electron beam. The simulations have shown that it is the best option to put the detectors as close as possible to reduce influence of the multiple scattering that plays important role for these energies.

After the real data were taken the simulation was used in order to estimate the telescopes resolutions. After alignment the residual distributions in the telescopes were calculated from the real data and from the simulations as well. The analysis of the measured telescope data was done by Kodyš [3], in this thesis we made the same analysis of the simulated data. In the simulation the spatial resolutions of telescopes were tuned so that the residual distribution widths from the simulation correspond to ones from the measurement for 3 GeV electrons. The obtained spatial resolutions are slightly different for each plane (see Table 9) and they fluctuate around 8.3 μm for Y-side and 8.0 μm for Z-side. To have a crosscheck of these values a method how to estimate the telescopes resolutions purely from the measured data was developed. It uses the most probable value l_{MPV} of the half-length of the confidence region of particle tracks. However, this method has its limits because it assumes that all the telescopes have the same resolutions. The estimated values of the telescopes resolutions using this method are (8.5 ± 0.1) μm on Y-side and (8.16 ± 0.10) μm on Z-side. The diference between these values and the arithmetic mean of the telescopes resolutions obtained from the simulation is lower or equal to 0.2 μm. We have used this comparison to estimate the accuracy of the telescopes spatial resolutions to be 0.4 μm.

Beside that other values such as the infinite energy extrapolation of the residual distribution widths in telescopes planes and the most probable half-length of the confidence region of tracks in DUT for all available energies were calculated from the measurements and the simulations as well. The difference between the measured and simulated values was lower or equal to 0.5 μm for the infinite energy extrapolation and lower or equal to 0.2 μm for the most probable half-length of the confidence region.

In order to determine the spatial resolution of DEPFET measurements for energies from 1 to 6 GeV were done. An effect of the multiple scattering can be than reduced by plotting square of the residual distribution width in DUT vs. the inverse square of energy and making the linear extrapolation to zero since the contribution of the multiple scattering is proportional to inverse energy. Beside that the contribution of the telescopes spatial resolutions in DUT plane must be known. The simulation was used in order to determine this value and a method how to calculate it without the simulation was developed as well (see formula (16)). The values calculated form the simulations are (4.25 ± 0.02) μm on Y side and (4.06 ± 0.02) μm on Z side, where the errors are the statistical ones obtained from the gaussian fit of the residual distribution – inaccuracy of the estimation of the telescopes resolutions wasn't taken into account. The values predicted from the measured data using the theoretical method are (4.32 ± 0.05) μm on Y side and (4.15 ± 0.05) μm on Z side. For the finite energy the contribution of the telescopes spatial resolution and the multiple scattering to the residual

distribution width in DUT can be calculated from the most probable value of the confidence region half-length using formula (19) that was found using the simulations. However this formula can be used only for the test beam layout that was used in January 2006 in DESY.

After that the spatial resolution of several DEPFET sensors was estimated. The analysis of DEPFET data was made by Velthuis et al. in [4]. They extrapolated the residual distribution widths measured in DEPFET plane to infinite energy that reduced the contribution of the multiple scattering. The contribution of the telescopes spatial resolution predicted by the simulation was then quadratically subtracted to determine DEPFET resolution. Obtained values are shown in Table 17.

Finally the dependence of the fraction of tracks that intersect the region of interest on its size was found, as it is shown in Figure 25 and in Appendix C. These plots are important when the efficiency and purity of the tested detector are calculated, since some hits can be shifted out of the region of the interest due to the multiple scattering.

Appendix A: used symbols

Width of residual distributions is inscribed with a symbol Δ:

$\Delta(dut)$ in DUT.

$\Delta(tel0)$, ..., $\Delta(tel3)$ in telescopes.

$\Delta^y(dut)$, $\Delta^z(dut)$ if it is necessary to distinguish y and z axis.

$\Delta_{tel}(dut)$, $\Delta_{ms}(dut)$ are the contributions of the telescopes spatial resolution and the multipple scattering in DUT.

$\Delta_{tel+ms}(dut)$ is total contribution of more effects.

$\Delta^y(dut, \infty)$ represents the infinite energy extrapolation of the residual distribution width in DUT.

Width of the error distributions of fitted points is inscribed with a symbol σ:

σ^y_{tel}, σ^z_{tel} are the spatial resolutions of the telescopes.

$\sigma^y_{tel_i}$ represents the spatial resolution of i-th telescope if it is not the same for all of them.

σ_{ms} is the contribution of the multiple scattering to the error distributions of fitted points.

$\sigma \equiv \sigma_{tel+ms}$ is the width of the error distribution that appears in theoretical equations.

$\sigma_{ms}(E)$ emphasis the explicit dependence on particle energy.

$\sigma^y(\infty)$ is again the infinite energy extrapolation.

Spatial resolutions of DUT are inscribed with symbols σ^y_{dut}, σ^z_{dut}

Confidence region half-length in DUT is inscribed with symbol l. Since in this paper only the value of l calculated in DUT plane is used, the detector specification (dut) is omitted.

l_{MPV} is the maximum probable value of the confidence region half-length l.

$l_{MPV}(\infty)$ is its infinite energy extrapolation.

Appendix B: derivations

In this appendix a derivation of several formulae is presented.

Formula (13): The half-length of the confidence region interval is defined as (see formula (8)):

$$l = t_{n-2}(\alpha) s \sqrt{Q_1}. \tag{21}$$

Note that the first two factors in formula (21) are constants. As Anděl describes in [10], $(n-k)s^2/\sigma^2$ is distributed according to χ^2_{n-k} distribution, where $n-k$ is number of degrees of freedom that equals 2 in our case and σ is a standard deviation of measured points y_i. Since half-length l

is proportional to the first power of s, χ^2_2 distribution function must be transformed using transformation described in [10] at page 48. If x is the random variable distributed according to the distribution function $f(x)$ and $y = t(x)$, where t is a strictly monotonous function with non-zero first derivative, then y is distributed according to $f(\tau(y))|\tau'(y)|$ where τ is the function inverse to t.

This transformation applied to l gives us:

$$\begin{aligned} 2\frac{s^2}{\sigma^2} \quad &\text{is distributed} \quad \chi^2_2\left(\frac{2s^2}{\sigma^2}\right), \\ s \quad &\text{is distributed} \quad \frac{4s}{\sigma^2}\chi^2_2\left(\frac{2s^2}{\sigma^2}\right), \\ l = cs \quad &\text{is distributed} \quad \frac{4l}{c\sigma^2}\chi^2_2\left(\frac{2l^2}{c^2\sigma^2}\right), \\ l \quad &\text{is distributed} \quad c_1 l\chi^2_2\left(\frac{l^2}{c_2^2}\right), \end{aligned} \tag{22}$$

where $c = t_2(\alpha)\sqrt{Q_1}$, $c_1 = 4/(c\sigma^2)$ and $c_2 = c\sigma/\sqrt{2}$. The function (22) has one maximum for $l = l_{MPV} = c_2$.

Formula (15): Assuming that the spatial resolution is the same for all the telescopes and if the particle is not scattered, the residual res_y in DUT plane can be calculated explicitly using formulas (6) and (12):

$$\begin{aligned} res_y &= \frac{\sum x_i^2 \sum y_i - \sum x_i \sum x_i y_i}{n\sum x_i^2 - \left(\sum x_i\right)^2} - \beta_0 \\ &= \sum \frac{\sum x_i^2 - x_i \sum x_i}{n\sum x_i^2 - \left(\sum x_i\right)^2} y_i - \beta_0. \end{aligned} \tag{23}$$

where x_i are the positions of the telescopes and y_i are the measured points of intersection. The coordinate system si chosen that in DUT $x = 0$. β_0 is the offset of the particle track that is equal to the real intersect position in this case. Random variables y_i are distributed according to Gaussian with the width σ_{tel}.

According to Anděl [10] the square of width of the residual distribution $\Delta^2_{tel}(dut)$ can be calculated as a sum of squares of the widths of the random variables error distributions that appear in formula (23):

$$
\begin{aligned}
(\Delta_{tel}(dut))^2 &= \sum \frac{\left(\sum x_i^2 - x_i \sum x_i\right)^2}{\left(n\sum x_i^2 - \left(\sum x_i\right)^2\right)^2}\sigma_{tel}^2 = \\
&= \sum \frac{\left(\sum x_i^2\right)^2 - 2x_i\sum x_i^2 \sum x_i + x_i^2\left(\sum x_i\right)^2}{\left(n\sum x_i^2 - \left(\sum x_i\right)^2\right)^2}\sigma_{tel}^2 = \\
&= \frac{n\left(\sum x_i^2\right)^2 - 2\sum x_i^2\left(\sum x_i\right)^2 + \sum x_i^2\left(\sum x_i\right)^2}{\left(n\sum x_i^2 - \left(\sum x_i\right)^2\right)^2}\sigma_{tel}^2 = \\
&= \frac{n\left(\sum x_i^2\right)^2 - \sum x_i^2\left(\sum x_i\right)^2}{\left(n\sum x_i^2 - \left(\sum x_i\right)^2\right)^2}\sigma_{tel}^2 = \\
&= \frac{\sum x_i^2\left(n\sum x_i^2 - \left(\sum x_i\right)^2\right)}{\left(n\sum x_i^2 - \left(\sum x_i\right)^2\right)^2}\sigma_{tel}^2 = \\
&= \frac{\sum x_i^2}{n\sum x_i^2 - \left(\sum x_i\right)^2}\sigma_{tel}^2 = G(x_1,\ldots,x_n)\sigma_{tel}^2. \qquad (24)
\end{aligned}
$$

Note that if $\sum x_i = 0$ (symmetric layout) the residual distribution width $(\Delta_{tel}(dut))^2 = \sigma_{tel}^2/n$.

Formula (16): According to formula (14) the telescopes spatial resolution can be calculated as

$$\sigma_{tel}^2 = \frac{2}{t_2(\alpha)Q_1}(l_{MPV}(\infty))^2, \qquad (25)$$

where $l_{MPV}(\infty)$ is the infinite energy extrapolation of the most probable value of the confidence region half-length and Q_1 is defined by formula (9)

$$Q_1 = \frac{1}{n} + \frac{(x-\bar{x})^2}{\sum x_i^2 - n\bar{x}^2}, \qquad (26)$$

where x is the position of DUT. If the coordinate system is chosen that $x = 0$, formula (25) can be written as:

$$
\begin{aligned}
\sigma_{tel}^2 &= \left(\frac{1}{n} + \frac{\bar{x}^2}{\sum x_i^2 - n\bar{x}^2}\right)^{-1}\frac{2}{(t_2(\alpha))^2}(l_{MPV}(\infty))^2 = \\
&= \left(\frac{\sum x_i^2 - n\bar{x}^2 + n\bar{x}^2}{n\sum x_i^2 - \left(\sum x_i\right)^2}\right)^{-1}\frac{2}{(t_2(\alpha))^2}(l_{MPV}(\infty))^2 = \\
&= \left(\frac{\sum x_i^2}{n\sum x_i^2 - \left(\sum x_i\right)^2}\right)^{-1}\frac{2}{(t_2(\alpha))^2}(l_{MPV}(\infty))^2. \qquad (27)
\end{aligned}
$$

Simple substitution to formula (24) gives us:

$$\Delta_{tel}(dut) = \frac{\sqrt{2}}{t_2(\alpha)}l_{MPV}(\infty). \qquad (28)$$

Appendix C: plots

In this section remaining plots that weren't presented in the text are shown. The plots aren't commented but it is possible to find at least one representative of each plot in the text.

Comparison of simulated and measured residual distribution widths in the telescopes

See Figure 13 and Figure 14 in the text for a description.

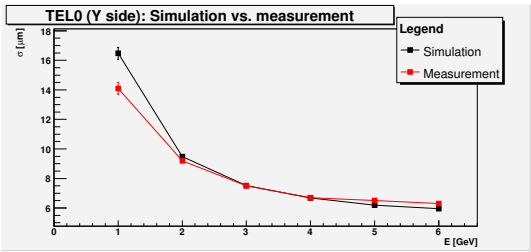

Simulation

Fract.	1 GeV	2 GeV	3 GeV	4 GeV	5 GeV	6 GeV
100 %	16.5 ± 0.4	9.48 ± 0.07	7.52 ± 0.04	6.67 ± 0.03	6.20 ± 0.03	5.96 ± 0.02

Measurement

Fract.	1 GeV	2 GeV	3 GeV	4 GeV	5 GeV	6 GeV
100 %	14.1 ± 0.4	9.2 ± 0.1	7.5 ± 0.1	6.7 ± 0.1	6.5 ± 0.1	6.3 ± 0.1

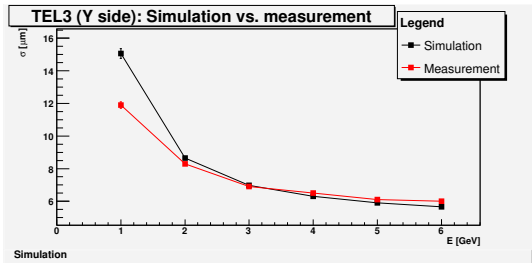

Simulation

Fract.	1 GeV	2 GeV	3 GeV	4 GeV	5 GeV	6 GeV
100 %	15.1 ± 0.3	8.65 ± 0.06	6.97 ± 0.03	6.31 ± 0.03	5.90 ± 0.02	5.66 ± 0.02

Measurement

Fract.	1 GeV	2 GeV	3 GeV	4 GeV	5 GeV	6 GeV
100 %	11.9 ± 0.2	8.3 ± 0.1	6.9 ± 0.1	6.5 ± 0.1	6.1 ± 0.1	6.0 ± 0.1

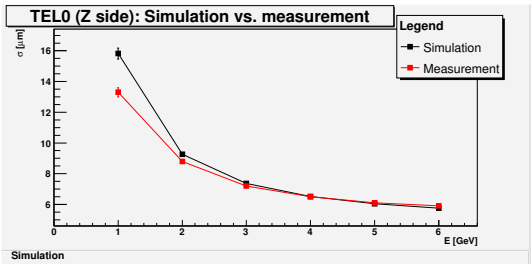

Simulation

Fract.	1 GeV	2 GeV	3 GeV	4 GeV	5 GeV	6 GeV
100 %	15.8 ± 0.4	9.27 ± 0.07	7.37 ± 0.04	6.51 ± 0.03	6.04 ± 0.02	5.75 ± 0.02

Measurement

Fract.	1 GeV	2 GeV	3 GeV	4 GeV	5 GeV	6 GeV
100 %	13.3 ± 0.3	8.8 ± 0.1	7.2 ± 0.1	6.5 ± 0.1	6.1 ± 0.1	5.9 ± 0.1

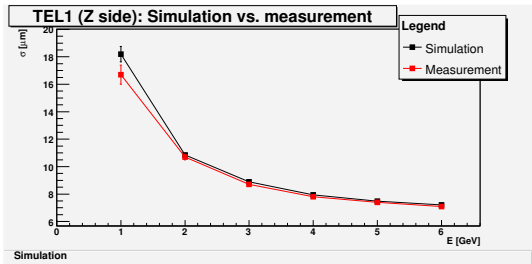

Simulation

Fract.	1 GeV	2 GeV	3 GeV	4 GeV	5 GeV	6 GeV
100 %	18.2 ± 0.6	10.8 ± 0.1	8.89 ± 0.06	7.95 ± 0.04	7.49 ± 0.04	7.22 ± 0.04

Measurement

Fract.	1 GeV	2 GeV	3 GeV	4 GeV	5 GeV	6 GeV
100 %	16.7 ± 0.7	10.7 ± 0.2	8.7 ± 0.1	7.8 ± 0.1	7.4 ± 0.1	7.1 ± 0.1

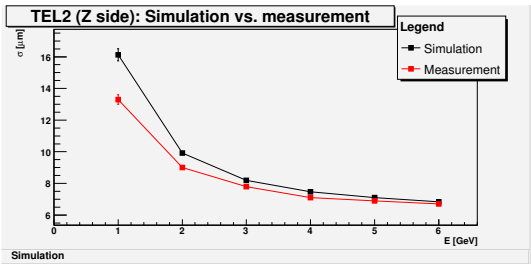

Simulation

Fract.	1 GeV	2 GeV	3 GeV	4 GeV	5 GeV	6 GeV
100 %	16.1 ± 0.4	9.92 ± 0.08	8.19 ± 0.05	7.47 ± 0.04	7.10 ± 0.03	6.84 ± 0.03

Measurement

Fract.	1 GeV	2 GeV	3 GeV	4 GeV	5 GeV	6 GeV
100 %	13.3 ± 0.3	9.0 ± 0.1	7.8 ± 0.1	7.1 ± 0.1	6.9 ± 0.1	6.7 ± 0.1

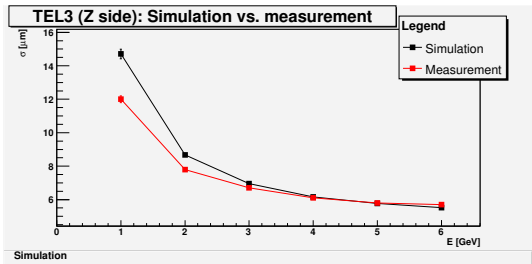

Simulation

Fract.	1 GeV	2 GeV	3 GeV	4 GeV	5 GeV	6 GeV
100 %	14.7 ± 0.3	8.68 ± 0.06	6.96 ± 0.03	6.16 ± 0.03	5.76 ± 0.02	5.52 ± 0.02

Measurement

Fract.	1 GeV	2 GeV	3 GeV	4 GeV	5 GeV	6 GeV
100 %	12.0 ± 0.2	7.8 ± 0.1	6.7 ± 0.1	6.1 ± 0.1	5.8 ± 0.1	5.7 ± 0.1

Comparison of the infinite energy extrapolation of the residual distribution width from the simulation and the measurement

See Figure 15 and Figure 16 in the text for a description.

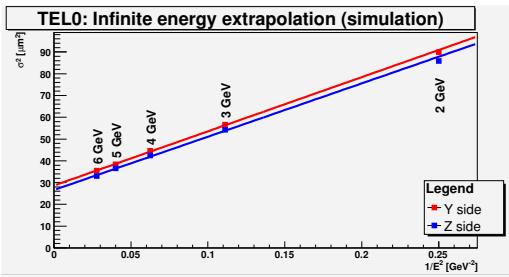

Linear extrapolation:	Y axis:	Z axis:
	$\sigma^2_{E\to\infty} = (28.6 \pm 0.2)\ \mu m$	$\sigma^2_{E\to\infty} = (26.6 \pm 0.2)\ \mu m$
	$\sigma_{E\to\infty} = (5.4 \pm 0.3)\ \mu m$	$\sigma_{E\to\infty} = (5.2 \pm 0.3)\ \mu m$

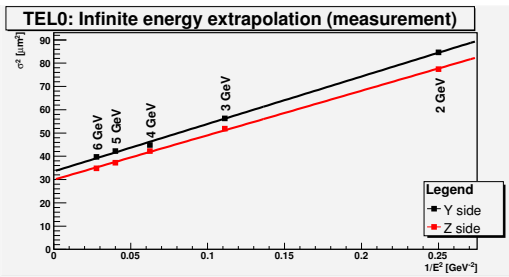

Linear extrapolation:	Y side	Z side
	$(\sigma^\infty_y)^2 = (33.50 \pm 0.10)\ \mu m$	$(\sigma^\infty_z)^2 = (29.91 \pm 0.10)\ \mu m$
	$\sigma^\infty_y = (5.8 \pm 0.1)\ \mu m$	$\sigma^\infty_z = (5.5 \pm 0.1)\ \mu m$

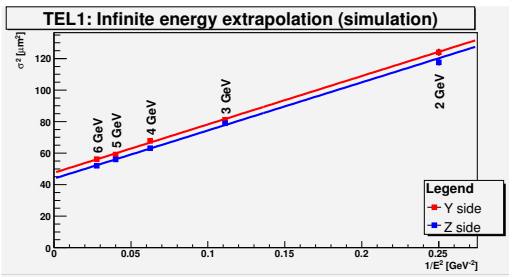

Linear extrapolation:	Y axis:	Z axis:
	$\sigma^2_{E\to\infty} = (47.5 \pm 0.4)\ \mu m$	$\sigma^2_{E\to\infty} = (43.8 \pm 0.4)\ \mu m$
	$\sigma_{E\to\infty} = (6.9 \pm 0.6)\ \mu m$	$\sigma_{E\to\infty} = (6.6 \pm 0.5)\ \mu m$

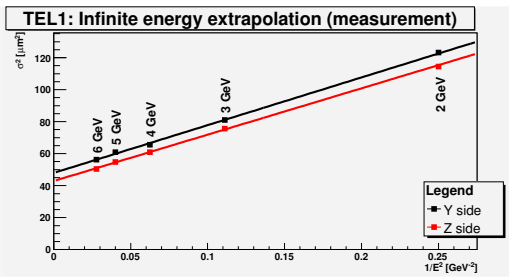

Linear extrapolation:	Y side	Z side
	$(\sigma^\infty_y)^2 = (47.9 \pm 0.1)\ \mu m$	$(\sigma^\infty_z)^2 = (42.9 \pm 0.1)\ \mu m$
	$\sigma^\infty_y = (6.9 \pm 0.2)\ \mu m$	$\sigma^\infty_z = (6.5 \pm 0.2)\ \mu m$

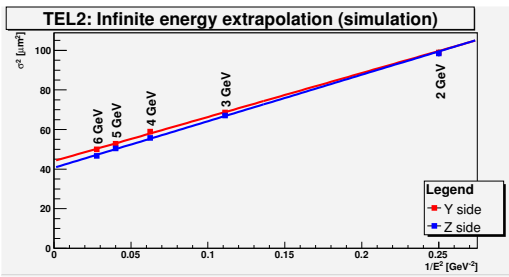

Linear extrapolation:	Y axis:	Z axis:
	$\sigma^2_{E\to\infty} = (44.1 \pm 0.3)\ \mu m$	$\sigma^2_{E\to\infty} = (40.7 \pm 0.3)\ \mu m$
	$\sigma_{E\to\infty} = (6.6 \pm 0.5)\ \mu m$	$\sigma_{E\to\infty} = (6.4 \pm 0.4)\ \mu m$

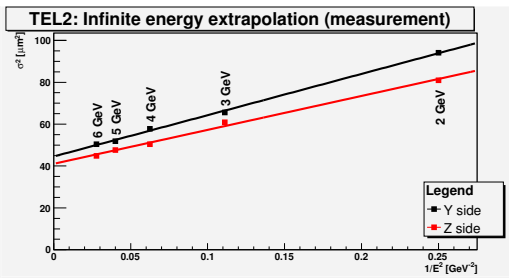

Linear extrapolation:	Y side	Z side
	$(\sigma^\infty_y)^2 = (44.56 \pm 0.10)\ \mu m$	$(\sigma^\infty_z)^2 = (41.00 \pm 0.10)\ \mu m$
	$\sigma^\infty_y = (6.7 \pm 0.1)\ \mu m$	$\sigma^\infty_z = (6.4 \pm 0.1)\ \mu m$

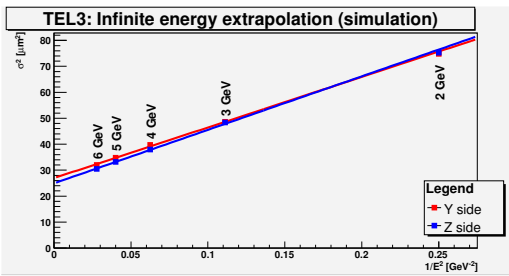

Linear extrapolation:	Y axis:	Z axis:
	$\sigma^2_{E\to\infty} = (27.0 \pm 0.2)\ \mu m$	$\sigma^2_{E\to\infty} = (24.9 \pm 0.2)\ \mu m$
	$\sigma_{E\to\infty} = (5.2 \pm 0.2)\ \mu m$	$\sigma_{E\to\infty} = (5.0 \pm 0.2)\ \mu m$

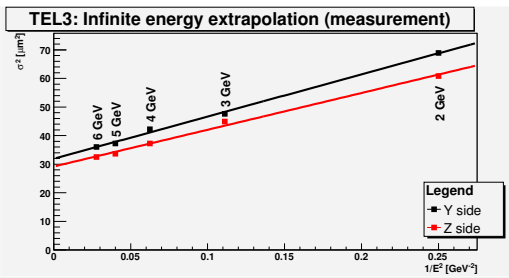

Linear extrapolation:	Y side	Z side
	$(\sigma^\infty_y)^2 = (31.89 \pm 0.10)\ \mu m$	$(\sigma^\infty_z)^2 = (29.17 \pm 0.10)\ \mu m$
	$\sigma^\infty_y = (5.6 \pm 0.1)\ \mu m$	$\sigma^\infty_z = (5.4 \pm 0.1)\ \mu m$

Energy dependency of the residual distribution width in DUT

See Figure 20 in the text for a description.

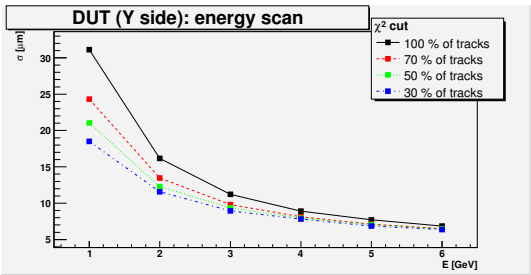

Fract.	1 GeV	2 GeV	3 GeV	4 GeV	5 GeV	6 GeV
100 %	31.1 ± 0.2	16.15 ± 0.08	11.21 ± 0.06	8.92 ± 0.05	7.70 ± 0.04	6.84 ± 0.04
70 %	24.3 ± 0.1	13.48 ± 0.08	9.80 ± 0.06	8.13 ± 0.05	7.10 ± 0.04	6.50 ± 0.04
50 %	21.1 ± 0.2	12.28 ± 0.08	9.35 ± 0.07	7.95 ± 0.06	7.06 ± 0.05	6.46 ± 0.04
30 %	18.5 ± 0.2	11.57 ± 0.10	8.95 ± 0.08	7.82 ± 0.07	6.85 ± 0.06	6.37 ± 0.06

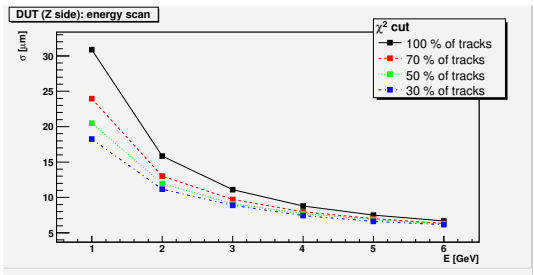

Fract.	1 GeV	2 GeV	3 GeV	4 GeV	5 GeV	6 GeV
100 %	30.9 ± 0.2	15.86 ± 0.08	11.11 ± 0.06	8.80 ± 0.04	7.51 ± 0.04	6.67 ± 0.03
70 %	23.9 ± 0.1	13.02 ± 0.07	9.71 ± 0.06	7.98 ± 0.05	7.02 ± 0.04	6.33 ± 0.04
50 %	20.5 ± 0.1	11.97 ± 0.08	9.13 ± 0.07	7.71 ± 0.06	6.89 ± 0.05	6.25 ± 0.05
30 %	18.2 ± 0.2	11.16 ± 0.10	8.89 ± 0.08	7.45 ± 0.07	6.63 ± 0.06	6.17 ± 0.06

Fraction of tracks that intersect ROI with specific size

See Figure 25 in the text for a description.

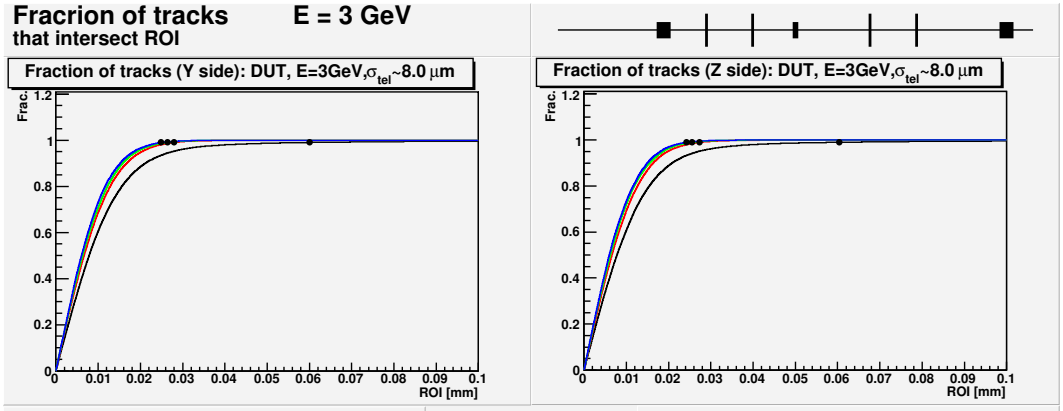

Fract.	$ROI_{99\%}$ (y) [μm]
100 %	60.06 ± 0.03
70 %	27.96 ± 0.03
50 %	26.44 ± 0.03
29 %	24.86 ± 0.03

χ² cuts
100 % of events
70 % of events
50 % of events
29 % of events

Fract.	$ROI_{99\%}$ (z) [μm]
100 %	60.42 ± 0.03
70 %	27.32 ± 0.03
50 %	25.56 ± 0.03
29 %	24.22 ± 0.03

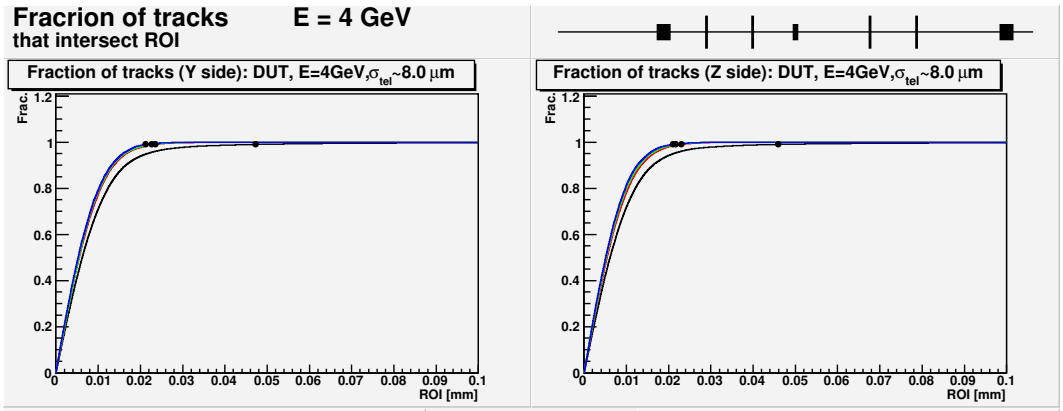

Fract.	$ROI_{99\%}$ (y) [μm]
100 %	47.26 ± 0.03
67 %	23.52 ± 0.03
47 %	22.62 ± 0.03
26 %	21.18 ± 0.03

χ² cuts
100 % of events
67 % of events
47 % of events
26 % of events

Fract.	$ROI_{99\%}$ (z) [μm]
100 %	45.90 ± 0.03
67 %	23.02 ± 0.03
47 %	21.68 ± 0.03
26 %	21.02 ± 0.03

Fracrion of tracks **E = 5 GeV**
that intersect ROI

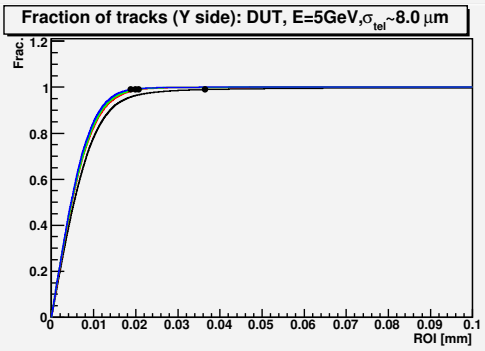

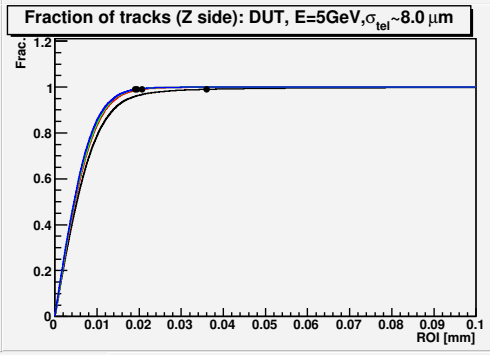

Fract.	$ROI_{99\%}$ (y) [μm]
100 %	36.42 ± 0.03
70 %	20.68 ± 0.03
50 %	19.96 ± 0.03
30 %	18.82 ± 0.03

χ^2 cuts
100 % of events
70 % of events
50 % of events
30 % of events

Fract.	$ROI_{99\%}$ (z) [μm]
100 %	36.04 ± 0.03
70 %	20.70 ± 0.03
50 %	19.48 ± 0.03
30 %	19.02 ± 0.03

Fracrion of tracks **E = 6 GeV**
that intersect ROI

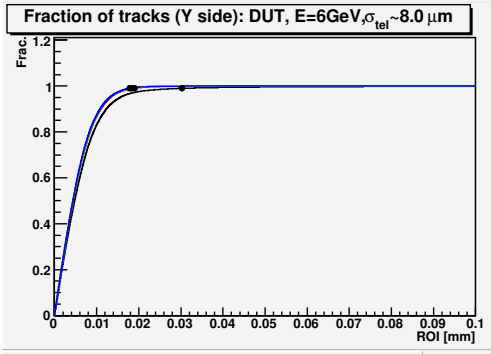

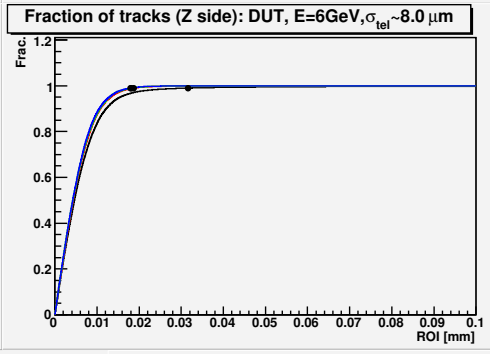

Fract.	$ROI_{99\%}$ (y) [μm]
100 %	30.24 ± 0.03
70 %	19.02 ± 0.03
50 %	18.38 ± 0.03
30 %	17.86 ± 0.03

χ^2 cuts
100 % of events
70 % of events
50 % of events
30 % of events

Fract.	$ROI_{99\%}$ (z) [μm]
100 %	31.64 ± 0.03
70 %	18.70 ± 0.03
50 %	18.20 ± 0.03
30 %	17.98 ± 0.03

References

[1] Particle Data Group: Review of Particle Physics, *The European Physical Journal C* **3** (1998), 1 – 794

[2] P. Kodyš: Data Evaluation in High Energy Physics Experiments, Study text for the lecture at Charles University, *http://www-ucjf.troja.mff.cuni.cz/... ...kodys/works/uceni/prednaska/ZpracovaniDatEn_11.pdf*, 2005

[3] P. Kodyš: Results of DEPFET test beam, *http://www-ucjf.troja.mff.cuni.cz/kodys/works/data_analysis/*, 2006

[4] R. Kohrs, H. Krüger, M. Mathes, L. Reuen, C. Sandow, M. Trimpl, J.J. Velthuis: Prelimeanry Results of the January testbeam, *Internal Note*, 2006

[5] D. Autiero, Y. Caffari, L. S. Esposito, A. Marotta, J. Marteau, P. Migliozzi: Characterization of the T24 electron beam line available at DESY, *http://adweb.desy.de/ testbeam/pictures/desytbfinal.pdf*, 2004

[6] J. Treis: Development and operation of a novel PC-based high speed beam telescope for particle tracking using double sided silicon microstrip detectors, *Dissertation, Universität Bonn*, 2002

[7] J. Treis, P. Fischer, L. Klingbeil, H. Krueger, N. Wermes, T. Lari: A modular PC based silicon microstrip beam telescope with high speed data acquisition *Nuclear Instruments and Methods in Physics Research* **A490** (2002) 112–123

[8] Geant 4 on-line documentation, *http://www.cern.ch/geant4*

[9] ROOT on-line documentation, *http://root.cern.ch/*

[10] J. Anděl: Základy matematické statistiky, *Matfyzpress*, Praha, 2005

[11] Home page of the DEPFET collaboration, *http://www.depfet.org*